UNIVERSITÄT DES SAARLANDES
NATURWISSENSCHAFTLICH-TECHNISCHE FAKULTÄT III
FACHRICHTUNG CHEMIE

Final Report

Applied Molecular Modelling

Frederik Philippi

23.10.2017

Table of Contents

1 Introduction

Chemistry can be interpreted as the science and art of “molecular engineering”, with the chemist being an engineer trying to manipulate the bonding, structure and interaction of Molecules. Due to the microscopic nature of chemistry, experimentally working chemists will never be capable to “see” what they are actually doing when manipulating molecules. Although there exists a vast variety of useful and widely applied models of what is happening inside a reaction vessel, it is nevertheless desirable to gain such an “insight”. Computational methods and quantum theory are of great help here: they provide tools to directly manipulate the reacting particles we are intrinsically unable to perceive. Another important advantage is that the exploration of exotic systems is more or less straightforward, even if they are impossible to prepare in an actual experiment.

To put it in a nutshell, almost every dynamic or static property can (or could) be calculated. In practice several constraints emerge from the complexity of the equations one has to solve and the computational effort needed even for small improvements. The challenge is hence to choose a suitable theoretical setup, which is able to include just the required features at a minimum amount of effort.

In this report, calculations on unsaturated bonds between heavy group 14 elements are presented, *i.e.* selected structural isomers of the disila-, digerma- and silagermabut-2-ynes as well as their fully fluorinated analogues. Although for a long time multiple bonds between heavier elements were believed to be unstable, they show indeed a rich chemistry, and even rather exotic heteronuclear heavier alkene homologues have been prepared experimentally.[1,2] Simple, small compounds incorporating heavy triple bonds are highly unstable and tend to oligo- or polymerise. Nevertheless, disilavinylidene, dimethyl disilavinylidene and their acetylene isomers are important model systems for theoretical studies concerning reactivity.[3–6] It was also shown that even silynes may be stable with sufficiently bulky substituents, although subtle effects like dispersion forces are important and smaller substituents problematic.[7–9] Besides providing kinetic protection, topology and steric demand of substituents also influence the relative stability of isomers. While it is established that the disilavinylidene structure is thermodynamically more stable for Si_2Me_2, this is no longer the case when methyl are replaced with supersilyl groups $Si(t\text{Bu})_3$, which favour a trans-bent structure.[10] The clever use of bulky

substituents thus provides the possibility to guide a reaction towards a certain desired structural motif, using both thermodynamic and kinetic effects.[11] Sekiguchi *et al.* put these findings into practise by synthesizing the first stable silyne and extensively studying its reactivity.[12–16]

Acetylene analogues can be reduced to dianions, which may also be interpreted as alkenes with two substituents being metal atoms. It was lately shown that reduction of a digermavinylidene to the corresponding dianion results in a substituent shift yielding a trans bent structure and *vice versa*. This issue was originally intended to be investigated and is dealt with in the preliminary calculations in chapter 1.1.[17]

Systematic studies concerning the influence of substitution pattern on molecular structure and properties require quantitative parameters that characterise different substituents. A commonly used approach in this sense are the Hammett parameters that are a measure for the ability of a substituent to withdraw or donate electron density by different mechanisms.[18] Consequently, eight substituents covering a broad and uniform range of Hammett sigma values were chosen and distributed to the participants of the course. The main part of this work deals with CH_3 and CF_3 as substituents.

Problems are expected to arise from the more electronegative substituents, because these are known to stabilize triplet states, at least for heavier heteroacetylenes.[19] Whereas dimethyl substituted disilavinylidene reportedly has a singlet ground state, this is no longer the case for NH_2, OH and F substituents.[20]

The electronic structure gives rise to “unusual” bending observed in multiple bonds of heavy elements, although the elements of the second period should be considered as the exception. According to the popular CGMT model, the observed trans bending is reasoned with the energy of the singlet-triplet splitting in the fragments obtained by homolytic bond dissociation relative to the bond energy gained by constructive interference.[21–23] If the singlet-triplet splitting is not overcompensated by bond energy as it is the case for carbon, the bond is formally composed of two singlet fragments. This leads to trans bending, by which Pauli repulsion is avoided and constructive overlap is made possible. Similar arguments apply for heavy alkynes and the doublet-quartet splitting of their fragments.[10,24,25] The presence of doubly bridged structures is usually traced back to electrostatic interactions.[26]

2 Computational Details

All calculations have been performed using the Gaussian 09 software package.[27] For the sake of simplicity, the term “global minimum” is sometimes used, which refers to the structure with the lowest energy out of those which were found. The term “stable” means “being a local minimum”. “Vinylidene” refers to the substituted disila-, digerma- or silagermavinylidenes as is obvious from the context. To facilitate reproduction of the results, important keywords for gaussian input files are given in brackets when appropriate. As is common practise, calculations were performed in absence of any electrical, magnetic or gravitational fields in a universe comprised of only the molecule of interest in the Born-Oppenheimer approximation, neglecting relativistic effects (besides spin) and gravitational interaction between the zero-dimensional particles as well as coupling between electronic states and molecular rotation, orbital movement *etc*.

Owing to the extremely flat potential energy surface characteristic for heavier group 14 elements, a decreased convergence threshold had to be used together with increased integral accuracy (opt=verytight int=ultrafine).[28] The steepest decent method (opt=steep) was used for geometries far from equilibrium or in other suitable cases as mentioned. IRC calculations were performed using a local quadratic approximation method (irc=LQA), which was also necessary due to the flat PES.[29] Furthermore, an increased step size together with a reduced convergence limit was employed during IRC (irc=(stepsize=30) iOP(1/7=5)). Other combinations of LQA with default values for method, step size and the convergence limit addressed by overlay 1/7 weren’t successful.

For TS searches, the use of symmetry was turned off (Symmetry=none). Unless stated otherwise, transition states were verified *via* intrinsic reaction coordinate calculation, subsequent optimization and comparison of the lowest normal mode eigenvalues. Starting geometries were generated from the educt and product geometries by choosing intermediate bond lengths, bond angles and dihedral angles or by using the quadratic synchronous transit methods implemented in gaussian (opt=qst2 and opt=qst3).[30] Structures from successful TS calculations for homologues were also used as input if available. It was furthermore possible to obtain several reasonable transition state structures from the two adjacent minimum geometries by eigenvector following in z-matrix, using at least the first five normal modes (opt=(EF,z-matrix)).

In cases where these methods failed, manual pseudo reaction coordinate searches – usually as relaxed scan or rigid z-matrix scan of two internal coordinates – were performed (opt=modredundant and scan=rigid).[31] In some cases the relaxed scan was performed in z-matrix, giving the possibility to employ more flexible restraints by the use of variables.

Natural bond orbital analysis, electrostatic charge fitting and Mulliken population analysis were performed in several cases (pop=(full,NBO,saveNBOs,ESP)).[32] Charges are given in units of one elemental charge. As initial guesses for the SCF input either the default method or an INDO guess (guess=INDO) were used. For unrestricted calculations, HOMO-LUMO mixing was requested (guess=(read,mix)). For chapter 3, the Gibbs free energy in kJ/mol is given together with the structures. The calculation of Gibbs free energy is based on the rigid-rotator-harmonic-oscillator and ideal gas assumptions and therefore very prone to artefacts and significant errors, which is why the SCF internal energy is also given in brackets.[30] There is also no account for hindered internal rotation, although necessary for rigorous calculations. Within any figure and therein type of energy, the species with the lowest energy is arbitrarily set to zero as reference.

The test for wavefunction stability implemented in gaussian (stable) was requested in several of the preliminary calculations in chapter 1.1. Minimum geometries obtained in the optimisations were checked for having a positive definite hessian and being a stationary point, *i.e.* having no residual gradients within the convergence limit.

Some calculations were run as unrestricted. In the majority of cases, this was necessary because analytical gradients are not available for restricted open shell calculations in gaussian. The use of numerical gradients increases the required amount of computational power and operator performance beyond the scope of this course, hence calculations involving an odd number of electrons had to be run as unrestricted. Due to the additional degrees of freedom, the energy of an unrestricted wavefunction may be lowered when compared to the restricted case. Occasionally this leads to significant spin contamination as higher spin states may be mixed into the resulting wavefunction. At least for stationary states, this is physically irrational. Usually the wavefunction collapses to the restricted (open shell) wavefunction, and as a measure for the extent of spin contamination, the eigenvalue of the square of the total spin is reported.[31,33] Acetylene, Si_2H_2 and $Li_2Si_2H_2$ were used as trial systems and are not further discussed.

3 Results and Discussion

3.1 Preliminary Calculations

Unless stated otherwise, all calculations in this subsection have been performed on unsaturated silicon-silicon species at the RB3LYP/6-311G(d,p) level of theory.

3.1.1 $Li_2Si_2Me_2$

Figure 1 shows the minimum geometries found for the $Li_2Si_2Me_2$ system, sorted into columns corresponding to their silicon-carbon-backbone. No instabilities were detected.

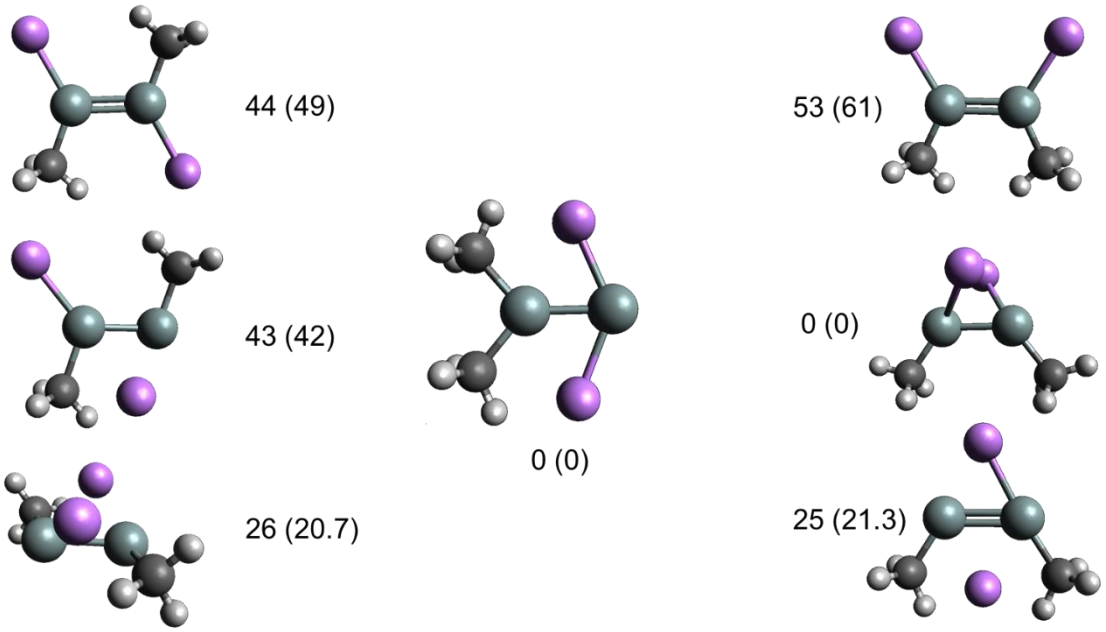

Figure 1: Structures for $Li_2Si_2Me_2$, with Gibbs free energies (internal energies) given.

The dianionic species in the left column are found to be less stable than the other two structures. The obvious mobility of the two lithium atoms leading to many minima causes problems due to the complexity of the PES and therefore the calculations involved when trying to describe transitions.

3.1.2 $LiSi_2Me_2$

As reasonable intermediate for the substituent shift which is expected when oxidizing the $Li_2Si_2Me_2$ presented in the preceding section, the neutral $LiSi_2Me_2$ radical was investigated. The structures obtained at the UB3LYP/6-311G(d,p) level of theory are shown in Figure 2. No further instabilities were detected.

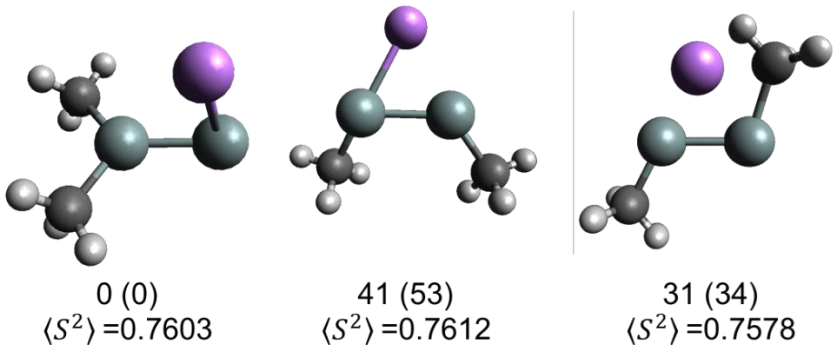

Figure 2: Structures for the $LiSi_2Me_2$ radical species, with Gibbs free energies (internal energies) and $\langle S^2 \rangle$ given.

Unlike for $Li_2Si_2Me_2$, the vinylidene structure is energetically favoured, although the influence of the lithium atom position was not investigated thoroughly.

Spin contamination is negligible, as the values for $\langle S^2 \rangle$ are close to $S(S+1)$. As a rule of thumb often employed, the deviation of $\langle S^2 \rangle$ from its physically expected value should be below 10%, which clearly is the case here.[31]

3.1.3 $Si_2Me_2^{2-}$

To avoid the problems arising from very mobile lithium atoms, calculations were also performed omitting the latter at the RB3LYP/aug-cc-pVTZ level of theory. The structures thus obtained are presented in Figure 3.

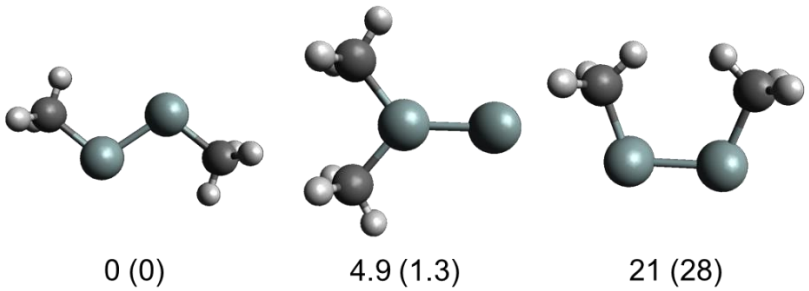

Figure 3: Structures for the dimethyl disilyne dianion, with Gibbs free energies (internal energies) given.

Although the differences in energy between vinylidene and disilyne were found to be small, the expected trend with the trans-bent structure being the most stable is reproduced. However, the results should be treated with care as for the trans-bent structure the first four occupied molecular orbitals were positive. For both trans-bent and vinylidene structure, the energy of the HOMO was +3.5 eV, i.e. the electron occupying the HOMO is only bound by the finite basis set. For the twisted cis bent structure, the energy

of the HOMO at this level of theory was +3.7 eV. These problems also occurred when using the Pople style basis set usually employed in this section, even after the addition of diffuse functions (6-311G(d,p) and 6-311++G(d,p)). Promising workarounds to the problem of negative electron affinity are addressed in the following subsections.

Out of the three relevant minima found, only for the vinylidene dianion a restricted/unrestricted instability was found, but the vertical distance in energy was found to be zero.

3.1.4 $Si_4H_6^{2-}$

For the purpose of stabilizing the dianion of the previous section, carbon was completely substituted with silicon. The structures obtained at the RB3LYP/aug-cc-pVTZ level of theory are shown Figure 4 and strongly resemble those shown in Figure 3.

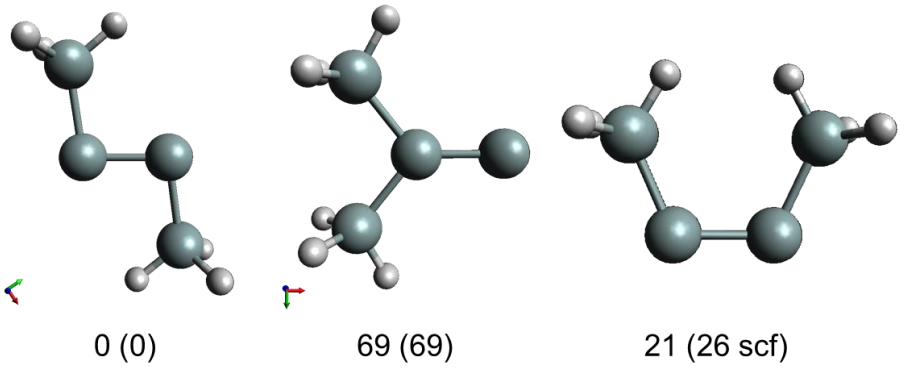

Figure 4: Structures for $Si_4H_6^{2-}$, with Gibbs free energies (internal energies) given.

The idea behind this was to take advantage of the well-known and experimentally observed capability of silicon to stabilize adjacent anions, at least carbanions.[34] Indeed, the HOMO energy is lowered to +3.0 eV for the trans-bent structure and +2.9 eV for the twisted cis bent structure, but the gain in stability is still insufficient.

Out of the three relevant minima found, only for the vinylidene dianion a restricted/unrestricted instability was found, but the vertical distance was found to be zero.

3.1.5 N-Heterocyclic Borylene Substituents

As the introduction of SiH_3 groups was not sufficient to stabilize the dianionic system with respect to electron detachment, N-heterocyclic borylenes (NHB) were examined as substituents, arriving at Si_2NHB_2 and $Si_2NHB_2^{2-}$. Selected geometries for the neutral species are shown in Figure 5, whereas Figure 6 shows the geometries for the dianion.

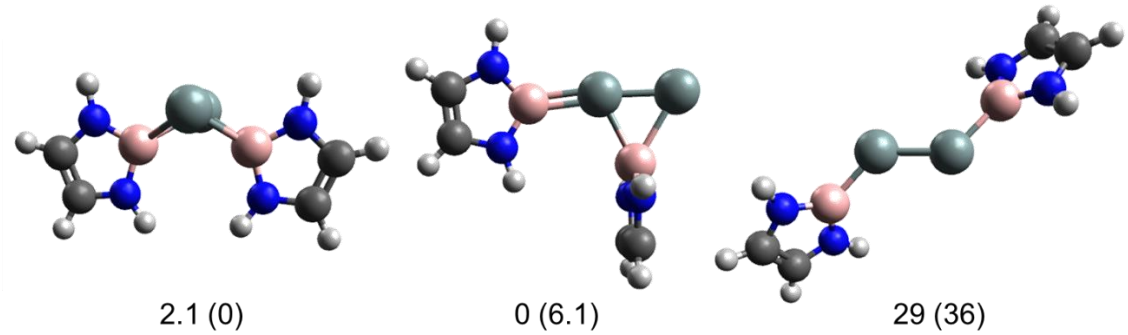

Figure 5: Structures for the neutral NHB substituted species, with Gibbs free energies (internal energies) given.

Rather unusual structures were found for the neutral system, the vinylidene being none of them. This was also one of the rare cases where the qualitative order of stability is different for the internal SCF energy and Gibbs free energy, with the internal energy being more trustworthy as discussed in the introduction.

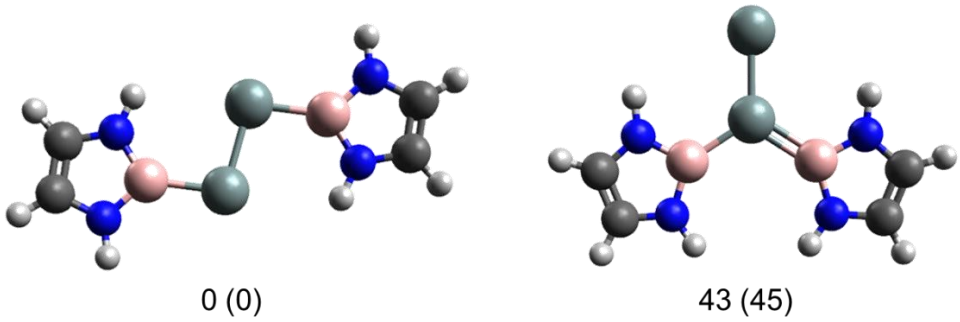

Figure 6: Structures for the dianionic NHB substituted species, with Gibbs free energies (internal energies) given.

For the case of the dianion, the trans-bent structure is the global minimum as expected, but still exhibits six positive occupied molecular orbitals, which is not acceptable.

3.1.6 Borole Substituents

For the sake of completeness, borole substituents were also considered as these have less electrons in the π system. Presumably due to the tendency of the latter for π-bonds/ -interactions, rather unusual structures were found like for the NHBs.

Geometries for the neutral species are presented in Figure 7.

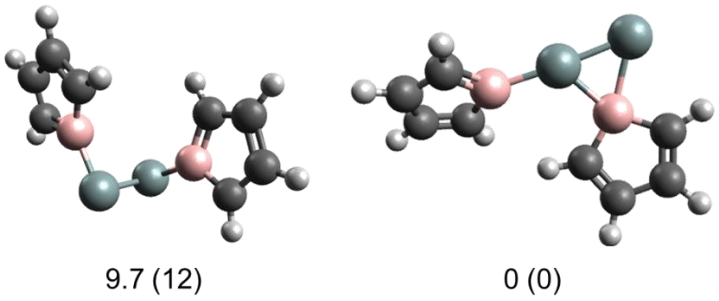

Figure 7: Structures for the neutral borylene substituted species, with Gibbs free energies (internal energies) given.

The left structure in Figure 7 exhibited an B-Si-Si-B dihedral angle of 94.6° and an B-Si-Si angle of 93.3°. The differences between the structures shown in the Figure 5 to Figure 8 indicate the presence of many interesting subtleties in the electronic structure, thereby a detailed wavefunction analysis may be a very rewarding task for future investigations.

Geometries for the dianion are shown in Figure 8.

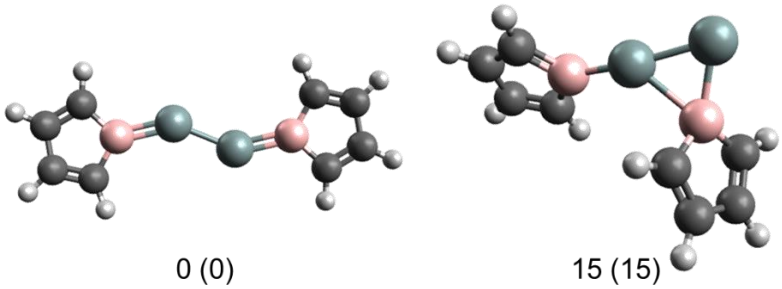

Figure 8: Structures for the dianionic borylene substituted species, with Gibbs free energies (internal energies) given.

The trans-bent structure is found to be more straight than usual, with an B-Si-Si angle of 144.9°. Average ESP (Mulliken) charges are −0.384 (0.092) on boron and 0.008 (−0.223) on silicon. The first six highest occupied orbitals are still positive.

3.1.7 Monophosphane Substituents

As the other methods presented in chapter 3.1.1 to 3.1.6 didn't deliver the success hoped for, not even with Hartree-Fock calculations with large basis sets containing many diffuse functions, it was concluded that the doubly negative charge has to be circumvented. Hence the emphasis was put subsequently on positively charged substituents. As the former dianion becomes neutral and the former neutral species becomes a dication, the problem of positive occupied orbitals is naturally circumvented. The dication species are in general also easier to converge, while maintaining a stable molecule. Several PMe_3

coordinated E_2 Species – including SiSi and GeGe – have been described in the literature in a very comprehensive study, although only focusing on trans-bent structures.[35] As first simple substituent, PH_3 was chosen. The structures for the resulting dication are shown in Figure 9.

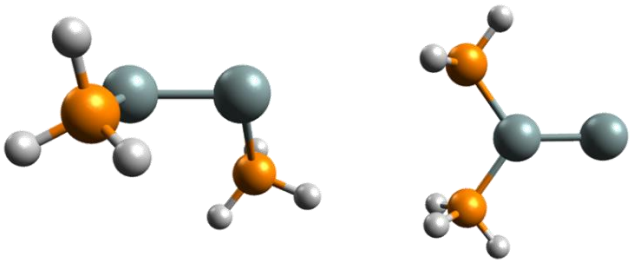

Figure 9: Structures for $Si_2P_2H_6^{2+}$, with Gibbs free energies (internal energies) given.

The trans-bent structure was found to collapse to a severely twisted structure with a P-Si-Si-P dihedral angle of 116.7°. As expected, the vinylidene structure is the more stable one. However, for the neutral species, which corresponds to the former dianion, the geometries shown in Figure 10 were obtained.

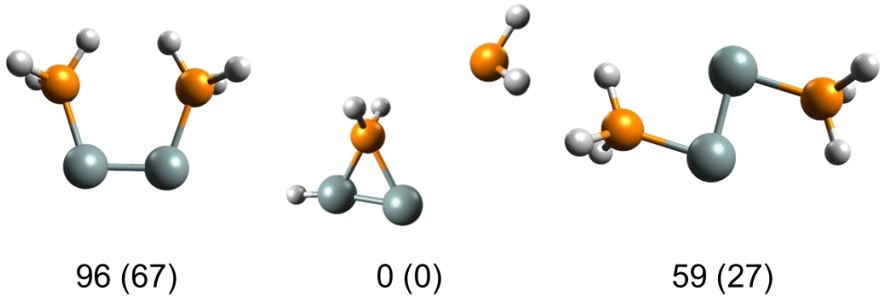

Figure 10: Structures for $Si_2P_2H_6$, with Gibbs free energies (internal energies) given.

Both a cis-bent and a trans-bent structure were found with P-Si-Si-P dihedral angles of 0.1° and 180.0°, respectively.

NBO analysis was performed for the trans-bent species to determine whether electronic structure correlates with molecular structure, especially the right angles. Figure 11 shows selected natural bond orbitals together with the atomic orbital contributions / hybridization on silicon for the trans-bent species.

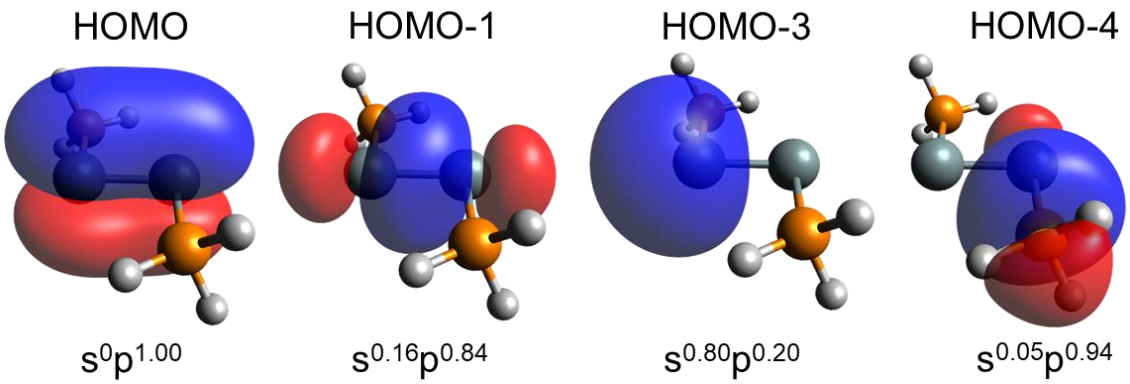

Figure 11: selected natural bond orbitals for $Si_2(PH_3)_2$ and hybridisation of silicon.

Phosphorus is substantially involved in the bonding situation in HOMO−4 with a valence electron configuration of $s^{0.39}p^{0.61}$ in the natural bond orbital. As this configuration is between the $s^{0.56}p^{0.44}$ configuration for the NBO lone pair in PH_3 analysed at the same level of theory and the ideal value of $s^{0.25}p^{0.75}$, the trans-bent species can be interpreted as a Si_2 unit stabilized by two PH_3 Molecules, which donate into empty p orbitals on Silicon. The natural bond orbitals support this rather simple interpretation, with HOMO to HOMO−3 belonging to two doubly bonded silicon atoms with one lone pair located on each of them.

Unexpectedly, the vinylidene input structures taken from previous calculations fragmented without observable barrier to the product shown in the middle column in Figure 10. This was even observed when smoothly optimizing using steepest decent (opt=steep) and small step sizes, so the possibility of overstepping a small barrier could be ruled out to some extent.

The Si_2PH_3 species arouse interest concerning its electronic structure, so a MCSCF calculation was set up using CASSCF[16,14]/6-311g(d,p)//RB3LYP/6-311G(d,p) in order to generate a more accurate wavefunction. As a method rather susceptible to erroneous input, all occupied valence orbitals should be included in the calculation as a full-valence MCSCF calculation is expected to be more robust with respect to a less experienced user. Hence [16,14]-CASSCF was chosen, which corresponds to full valence SCF and circumvents some of the “many subtleties” of this “powerful but advanced” method.[36] Only orbitals 21 and 22 had to be permuted manually (guess=alter). With this setup, not only all occupied valence orbitals, but also the relevant virtual orbitals are included in a symmetrical manner (i.e., both P-H σ* orbitals should be included, not only one) Figure 12

shows the electrostatic potential mapped onto the 1 me/Å^3 isosurface of the obtained electron density together with a proposed Lewis resonance structure based on common phosphonium species. Although one would intuitively expect a negative charge on silicon and a positive charge on phosphorus, the ESP plot proves this assumption wrong. Mulliken analysis also puts a negative charge of −0.03 on phosphorus. An AIM analysis is expected to provide further insight into bonding and charge distribution, but was not pursued at this stage of the calculations.

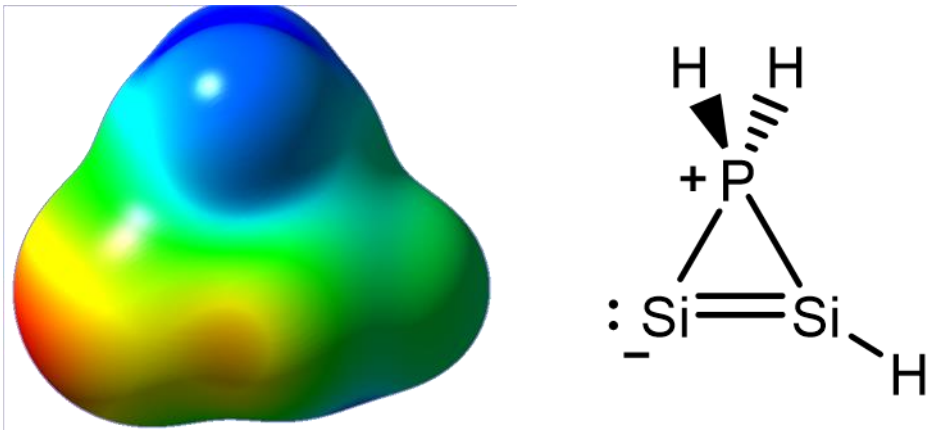

Figure 12: ESP plot (red = high / blue = low potential energy of positive test charge) and Lewis formula of Si_2PH_3.

Table 1 lists the occupancies obtained via NBO analysis, together with the ones obtained at the RHF/6-311G(d,p)//RB3LYP/6-311G(d,p) level of theory for comparison.

Table 1: Natural bond orbital occupancies for selected orbitals of the Si_2PH_3 species.

	CASSCF		**RHF**	
	bonding	**antibonding**	**bonding**	**antibonding**
Si-Si σ-bond	1.93	0.04	1.97	0.00
Si-Si π-bond	1.73	0.09	1.81	0.00
P-H σ-bonds	1.97	0.13	1.98	0.10
Si lone pair	1.95	/	1.98	/

The effect of donation into the P-H σ* orbitals is much less pronounced than expected, but still visible. It is furthermore obvious that only little is gained when passing on to CASSCF.

3.1.8 $P(SiH_3)_3$ Substituents

To avoid the rearrangement observed for $Si_2P_2H_6$, all hydrogens were substituted with SiH_3 groups. Figure 13 shows the geometries found for the dication.

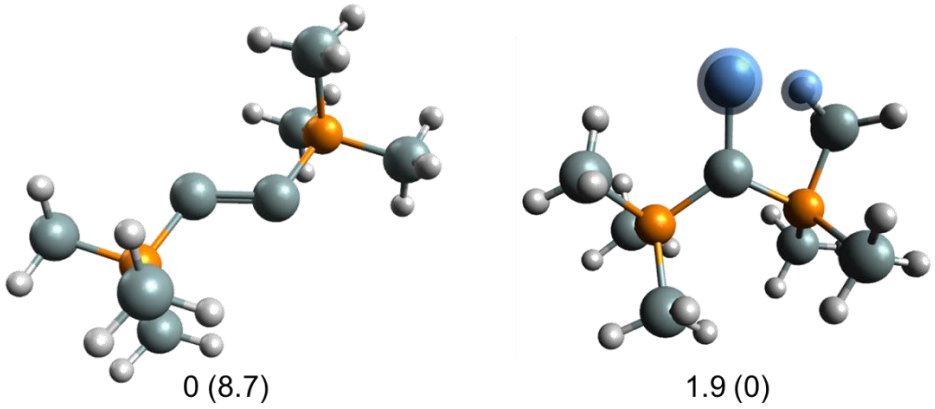

Figure 13: Structures for $Si_2P_2(SiH_3)_6^{2+}$, with Gibbs free energies (internal energies) given.

The two relevant structures are rather close in energy, so that the relative order is different for Gibbs free energy and internal SCF energy. Interestingly, one of the SiH_3 units approaches the silicon atom which is marked blue in Figure 13, so the Si-H-bond between the two marked atoms is with 1.83 Å only 18% longer than the plotted Si-H-bond of the SiH_3 group. In order to get insight into the bonding situation, a contour plot through the Si-Si-P-plane is shown in Figure 14.

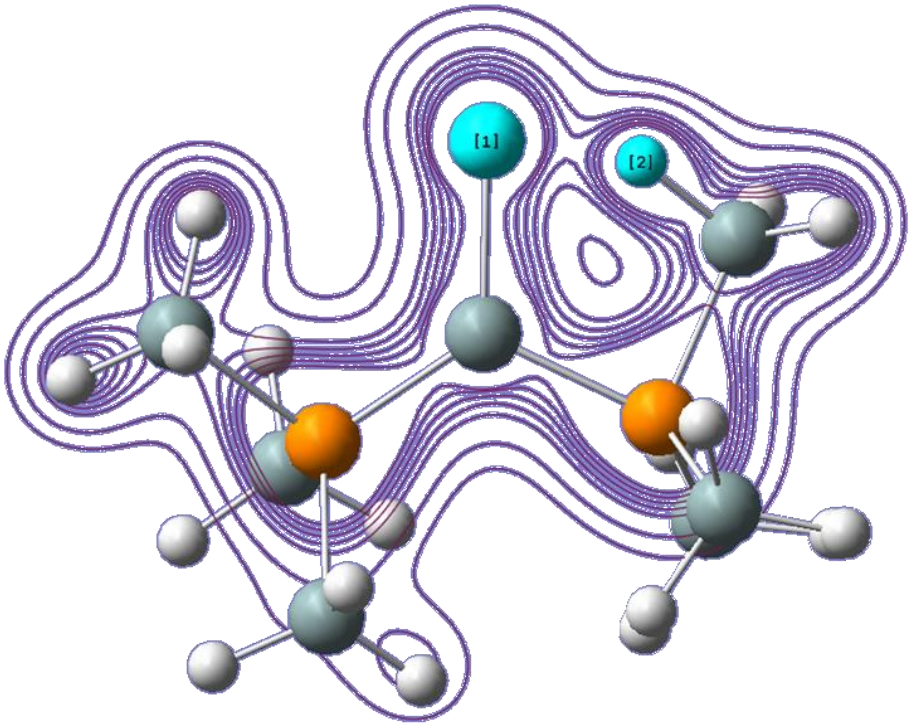

Figure 14: Contour plot of the electron density for the $Si_2P_2(SiH_3)_6^{2+}$ vinylidene structure.

Although the electron density between atoms 1 and 2 is rather large, it doesn't reach the usual bond density. Average ESP (Mulliken) charges on silicon 1 are 0.354 (0.415) and on hydrogen 2 −0.180 (−0.135). The interaction therefore appears to be mainly electrostatic.

The geometries for the neutral Species are shown in Figure 15.

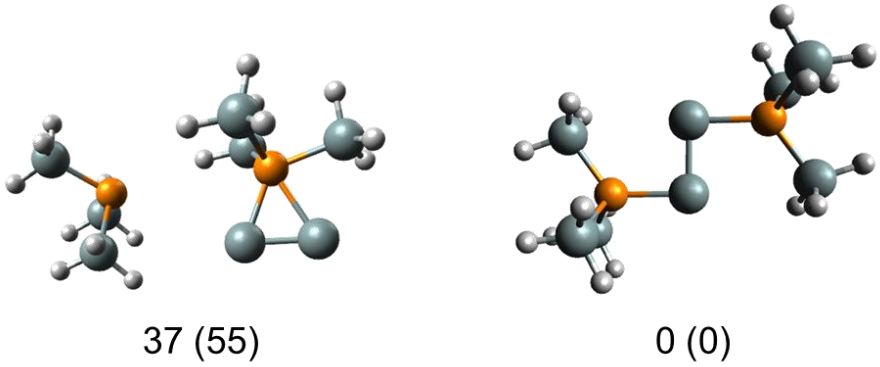

Figure 15: Structures for $Si_2P_2(SiH_3)_6$, with Gibbs free energies (internal energies) given.

Although one phosphine group is still eliminated, no SiH_3 group is transferred when optimizing vinylidene starting structures. The trans-bent species exhibits a rather unusual structure, with a P-Si-Si-P dihedral angle of 180.0° and an P-Si-Si angle of 90.5°. Average ESP (Mulliken) charges on phosphorus are −0.525 (−0.651), on the two central silicon atoms −0.099 (0.010) and on the remaining silicon atoms 0.783 (0.513). These charges support the interpretation of the trans-bent species as a neutral Si_2 unit which is stabilized/coordinated by two phosphine molecules, as was found for $Si_2(PH_3)_2$.

3.1.9 NHC Substituents

N-heterocyclic carbenes were chosen as a promising substituent combining positive charge and electronic stabilization. Indeed, similar compounds have already been prepared experimentally.[37] Especially the related $cAAC_2Si_2$ and NHC_2Si_2 are well examined, and even redox chemistry has been realised with NHC_2Si_2.[38–40]

Calculations were performed using the simplest NHC, with the results for the dication shown in Figure 16. Sterically more demanding groups were excluded because of the increased computing demand.

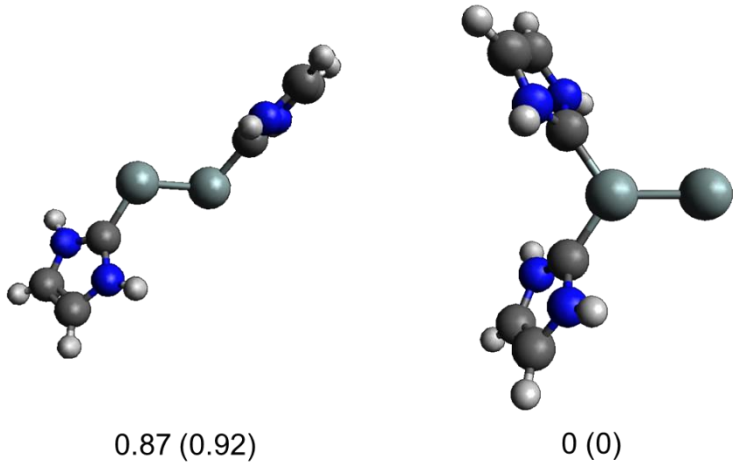

Figure 16: Structures for $Si_2NHC_2^{2+}$, with Gibbs free energies (internal energies) given.

The trans-bent structure is found to be only 1 kJ/mol higher in energy and is thus within reach of thermal energy. It can easily be understood that the trans-bent structure becomes favourable when employing the sterically demanding groups that are required to prevent side reactions like dimerization. Figure 17 shows the structures found for the neutral species.

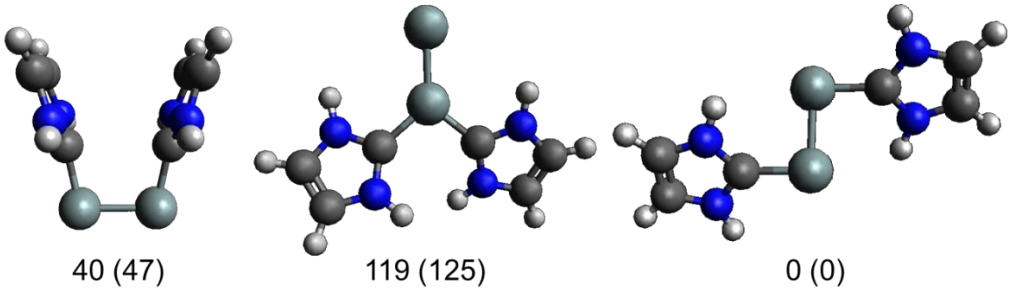

Figure 17: Structures for Si_2NHC_2, with Gibbs free energies (internal energies) given.

Both the vinylidene and trans-bent structure resemble the ones found for the borole substituents in 3.1.5, only the structure on the left is unprecedented. Again, a C-Si-Si angle which is with 92.5° almost rectangular has been found in the trans-bent structure.

3.1.10 Aryl Substituents

Representing aryl substitution, phenyl groups were chosen as model compound. Geometries were calculated only for the neutral species and are shown in Figure 18.

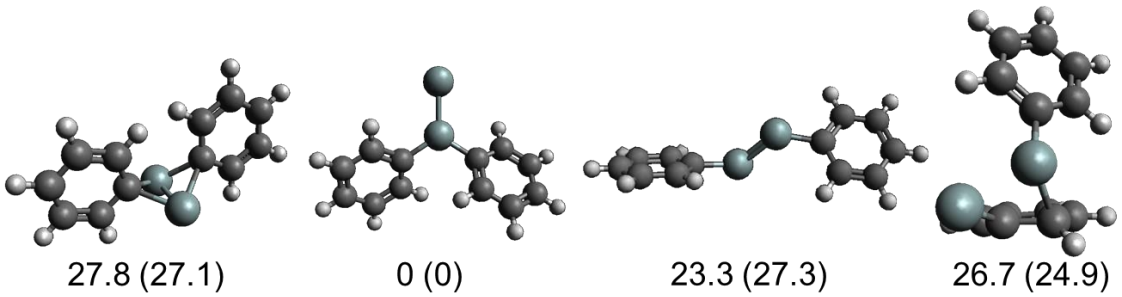

Figure 18: Selected structures for Si_2Ph_2, with Gibbs free energies (internal energies) given.

A twisted disila vinylidene was found to be the global minimum. The distorted structure shown on the right in Figure 18 was found to be comparable in energy with the doubly bridged structure on the left. The latter showed nearly no sign of the expected steric interaction between the hydrogen atoms in close proximity. Both bonds from one of the carbon atoms not connected to hydrogen to the two silicon atoms are basically of the same length, differing only about two percent or 0.05 Å.

To force the diphenyl system into a bridged structure, the system shown Figure 19 with a methylene group connecting the two phenyl rings was also investigated.

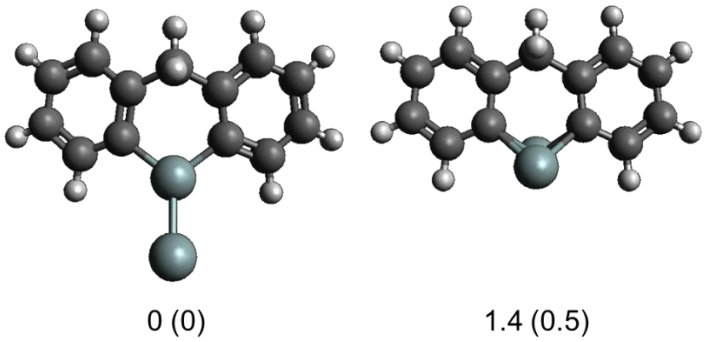

Figure 19: bridged / vinylidene Si_2 diphenylmethane species, with Gibbs free energies (internal energies) given.

By introduction of the bridging group, the difference between both species becomes negligible compared to thermal energy (about 2.5 kJ/mol at room temperature), although the height of the barrier separating the two minima was not further investigated. With sterically demanding groups at the place of the hydrogen atoms neighbouring the reactive Si_2 centre, similar compounds might be interesting synthetic targets. The doubly bridged species on the right was found to be unstable as dianion.

3.1.11 Dimethyldisilyne Si_2Me_2 Isomers

The dimethyldisilyne dealt with in this chapter serves as a model compound for alkane substituted heavier alkyne isomers and is occasionally studied in the literature. This system was also chosen for further investigation in chapter 3.2.1. The stable structures found at this point are presented in Figure 20.

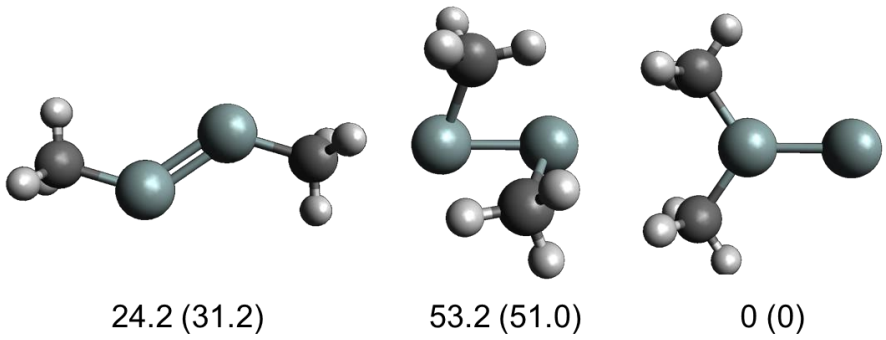

Figure 20: Structures for dimethyldisilyne, with Gibbs free energies (internal energies) given.

As anticipated, the vinylidene is energetically favoured by a clear margin. The wavefunction stability tests indicated a restricted/unrestricted instability for the vinylidene, and a vertical (adiabatic) difference in the internal SCF energy of 1.9 (2.1) kJ/mol was found. Therefore, correlated methods which are able to account for diradical character may be necessary.

The geometry for the twisted bridged structure was reported differently in the literature and is close to the right one shown Figure 21, whereas the left picture shows the structure obtained in this work.

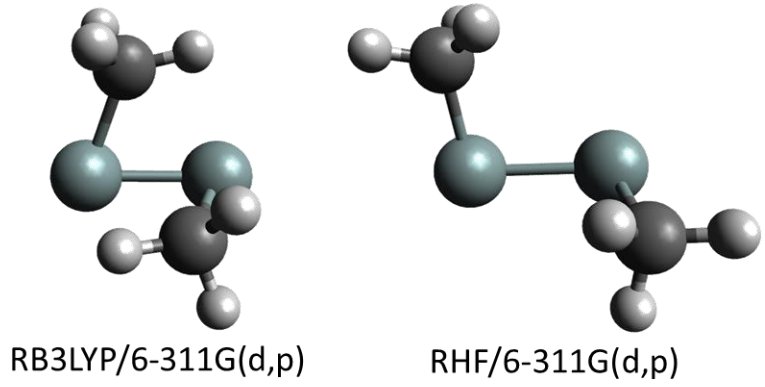

Figure 21: Minimum geometry of dimethyldisilyne twist structure at different level of theory.

Because of the remarkable differences in bond angles and the rotational orientation of the methyl groups, optimizations were performed at different levels of theory. The results are given in Table 2.

Table 2: Selected geometrical parameters of bridged / twisted dimethyldisilyne at different level of theory.

Level of theory	Si-Si-C angle	Si-Si bond	Si-C bond	C-Si-Si-C dihedral
RB3LYP/6-311G(d,p)	71.4°	2.282 Å	1.997 Å	94.5°
RB3LYP/aug-cc-pVQZ	71.0°	2.268 Å	1.990 Å	95.1°
RHF/6-311G(d,p)	98.4°	2.392 Å	1.928 Å	96.8°
RMP2/6-311G(d,p)	67.7°	2.259 Å	1.989 Å	93.5°
HF/DZ+PP[41]	99.9°	2.378 Å	1.928 Å	97.2°
RCCSD/6-311G(d,p)	71.2°	2.280 Å	1.977 Å	92.5°
RBD/6-311G(d,p)	71.2°	2.280 Å	1.977 Å	92.5°

The larger angles seem to be an artefact of the Hartree-Fock calculations, as both the B3LYP hybrid functional and the correlated methods produce consistent geometrical parameters. It should be mentioned that the twist structure itself as a stable minimum was considered to be an artefact of HF in the literature.[41,42] This is probably because the geometry therein obtained was used as input for a rather sophisticated correlated method. Using the RHF/6-311G(d,p) geometry shown on the right in Figure 21 as input for the calculation with RB3LYP/6-311G(d,p) indeed yielded a trans-bent species. Analysis using the AIMAll solution on the RCCSD-FC/6-311G(d,p) wavefunction yielded AIM charges of 0.671 (−0.666) on silicon (carbon) atoms.[43] The electrostatic nature of the doubly bridged structure is apparent from these values. NBO charges are comparable with 0.467 (−1.074) on silicon (carbon) atoms, the same holds true for Mulliken charges with 0.288 (−0.670) on silicon (carbon) atoms. However, ESP charges are qualitatively different with −0.161 and −0.168 (0.876 and 0.997) on silicon (carbon) atoms. As indicated by the rather different values within each of the two sets of symmetrically equivalent atoms, this might be an artefact of the employed ESP fitting scheme.

Analytical second derivatives are not available for Brueckner Doubles, so the bridged structure given in Table 2 has been (successfully) confirmed being a minimum by using a numerically generated hessian (freq=(numerical,FourPoint)).

Among the two simulations using the hybrid functional, only marginal changes are observed. The choice of theory has a crucial influence on the output, as due to the very flat PES, only little energy difference is required for large changes in the geometry.

Another issue is the electronic structure of the disilavinylidene, first of all whether the ground state is a singlet or triplet. Several combinations of method and basis set were employed, with the results given in Table 3.

Table 3: Singlet-triplet splitting for the disilavinylidene isomer of dimethyldisilyne at different levels of theory.

Level of theory	ΔE_{S-T}	$\langle S^2 \rangle$ **(triplet)**
UHF/6-311G(d,p)	−40.8 kJ/mol	2.0262
R(O)HF/6-311G(d,p)	−28.1 kJ/mol	
ROMP2/6-311G(d,p)	11.5 kJ/mol	
UHF/aug-cc-pVTZ	−43.7 kJ/mol	2.0375
UHF/aug-cc-pVQZ	−44.1 kJ/mol	2.0384
R(O)B3LYP/6-311G(d,p)	+21.3 kJ/mol	
R(O)B3LYP/aug-cc-pVTZ	+20.8 kJ/mol	
B3LYP/ aug-cc-pVTZ[20]	+12.1 kJ/mol	

Hartree-Fock methods seem to be less reliable, whereas the influence of the basis set is much less pronounced. UB3LYP calculations yield even higher singlet-triplet-splitting.

Significant diradical character is reported for trans-bent Ge_2Me_2 and Si_2Me_2 in the literature, which is not described by RB3LYP.[30,44] An additional NBO analysis at the [8,8]-CASSCF/6-311g(d,p)//RB3LYP/6-311G(d,p) level of theory was performed for the vinylidene, but due to disk space limitations, full valence CASSCF was impractical, so the results have to be treated with care. The greatest change observed when compared to RHF/6-311G(d,p)//RB3LYP/6-311G(d,p) was a decrease of the bond order of the Si-Si-π-bond from 0.98 to 0.89.

For this particular system, transition states connecting adjacent isomers were found and verified. The resulting energy profile is shown in Figure 22.

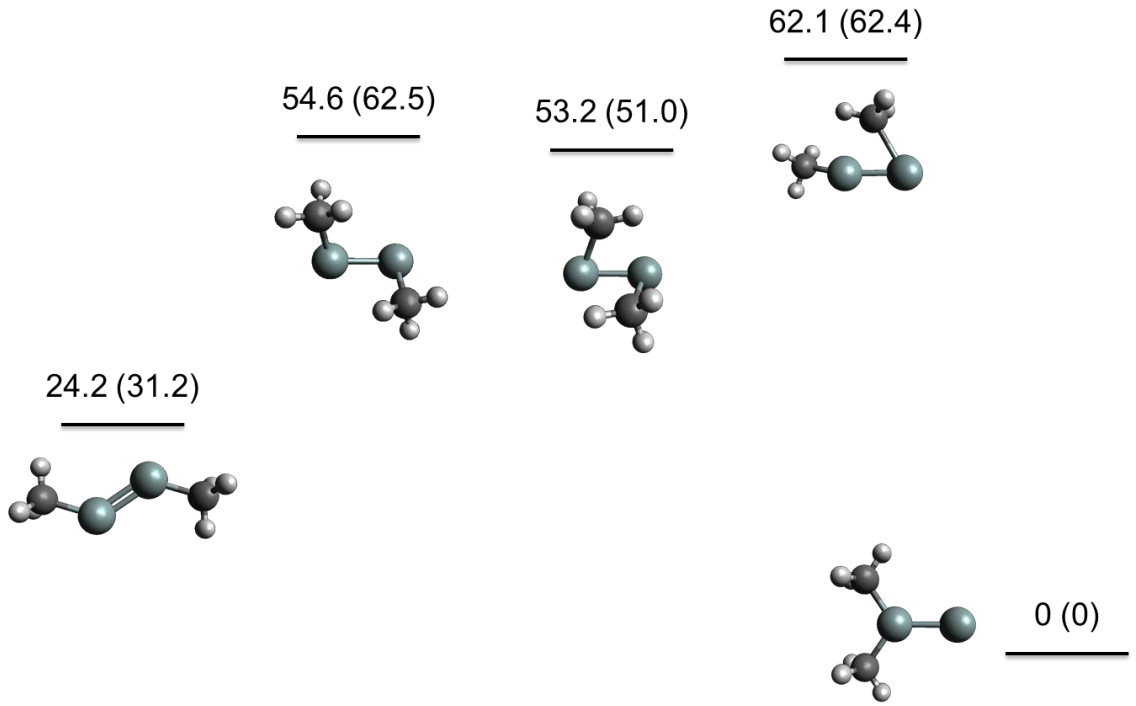

Figure 22: Energy profile for the isomerisation of dimethyldisilyne, with Gibbs free energies (internal energies) given.

The seemingly small barrier for the isomerization from bridged to trans-bent has to be treated with care, as the vertical distances are based on Gibbs free energies.

3.2 Final Calculations

Unless stated otherwise, calculations presented in this subsection are performed at the RB3LYP/cc-pVTZ level of theory. Transition states are verified using IRC and subsequent optimization as stated in chapter 2. Within any of the figures showing energy profiles, the vertical positions of the black bars attached to each species are proportional to its internal SCF energy. The latter is given in units of kJ/mol to one decimal place.

The nomenclature is as follows: The name of the molecule is comprised of the symbols of the two central atoms, *i.e.* Si or Ge, followed by 'GS' for ground states and 'TS' for transition states and a number characterising the structure. Trans-bent structures have the number '1', the doubly bridged / twisted structures have the number '2', and number '3' is reserved for vinylidenes. In the case of heteronuclear vinylidenes, the atom connected to the carbon substituents is named first. Transition states are characterized by two numbers, depending on the two structures connected by the transition state.

3.2.1 Isomers of $E_2(CH_3)_2$

Selected geometrical quantities of the trans-bent and bridged isomers of E_2Me_2 are listed in Table 4. For the heteronuclear species, the second angle given is always the Si-Ge-C angle. E-E bond lengths and E-E-C angles for the vinylidene isomers can be found in Table 7 in chapter 3.2.2.

Table 4: Selected geometrical parameters of dimethyldisilyne isomers.

System	C-E-E-C Dihedral	E-E-C Angle	E-E Bond
SiSiGS1	180°	129.2°	2.118
SiGeGS1	180°	128.2° / 128.1°	2.176
GeGeGS1	180°	127.2°	2.238
SiSiGS2	95.0°	71.1°	2.274
SiGeGS2	94.7°	74.4° / 67.8°	2.345
GeGeGS2	71.0°	94.6°	2.414

Because of the larger core of germanium, the increasing E-E bond length in each of the SiSi / SiGe / GeGe series is not surprising. The decreasing dihedral angle can similarly be rationalized with the decreased steric interaction between the methyl groups due to large bond lengths and E-E-C angles. To provide a short glimpse on the electronic structure of the vinylidene, Table 5 lists hybridisation / orbital contributions on the isolated Si or Ge atom not connected to carbon obtained by means of natural bond orbital analysis.

Table 5: Atomic orbital contributions / hybridization for remote Si or Ge from NBO analysis.

System / Atom	E-E Bond 1	E-E Bond 2	Lone Pair
SiSiGS3 / Si	$s^{0.14}p^{0.86}$	$s^{0.00}p^{1.00}$	$s^{0.87}p^{0.13}$
SiGeGS3 / Ge	$s^{0.11}p^{0.89}$	$s^{0.00}p^{1.00}$	$s^{0.89}p^{0.11}$
GeSiGS3 / Si	$s^{0.12}p^{0.88}$	$s^{0.00}p^{1.00}$	$s^{0.89}p^{0.11}$
GeGeGS3 / Ge	$s^{0.09}p^{0.91}$	$s^{0.00}p^{1.00}$	$s^{0.91}p^{0.09}$

The well-known trend of heavier elements preferring p-orbitals in their bonding is clearly visible, as is the increasing s-character of the lone pair. These results also partly explain why the Ge-Ge-C angle is much closer to 90° than the Si-Si-C angle in the bridged species.

3.2.1.1 Silicon-Silicon

Figure 12 shows the energy profile for the isomerization of Si_2Me_2. The lengths of the Si-Si bond as well as the Si-C bond lie between the ones reported in the literature, with a deviation of less than 2%; the deviation of the Si-Si-C angle from the literature values is below 1%.[42,45]

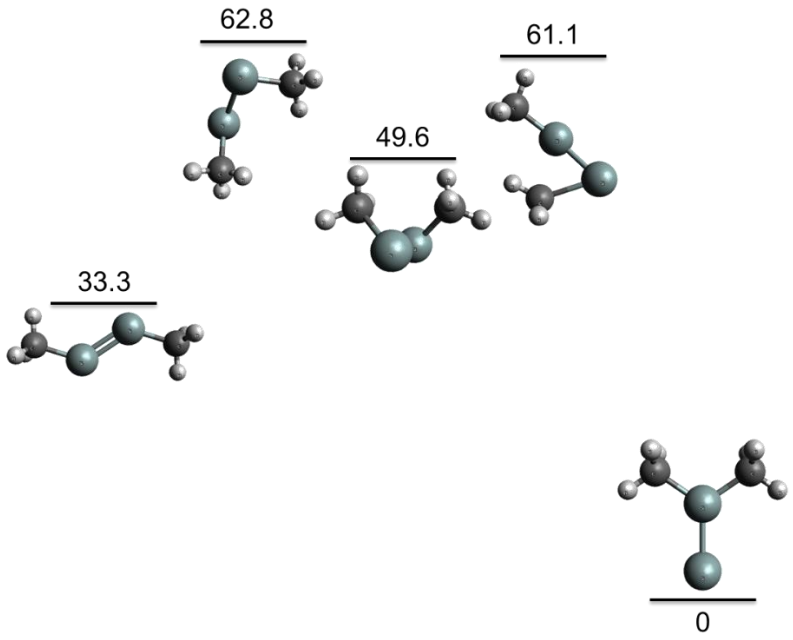

Figure 23: Energy profile for the isomerisation of Si_2Me_2, with internal energies given.

The doubly bridged species is again found to be a true minimum, with considerable barriers towards activation. So far, the literature finding of the GS2 structures not being minima is not comprehensible. Obtained energies and barriers are basically identical to the internal energies given in the energy profile in Figure 22, which were obtained with a Pople style triple zeta basis set instead of the correlation-consistent basis set used in the final calculations.

As illustrated in Chapter 3.1.11 using energies and geometrical parameters, the basis set influence is negligible, and neither a larger basis set nor a more sophisticated method beyond B3LYP seems to be required to produce reliable geometries.

3.2.1.2 Silicon-Germanium

The energy profile for the $SiGeMe_2$ isomerisation is shown in Figure 24.

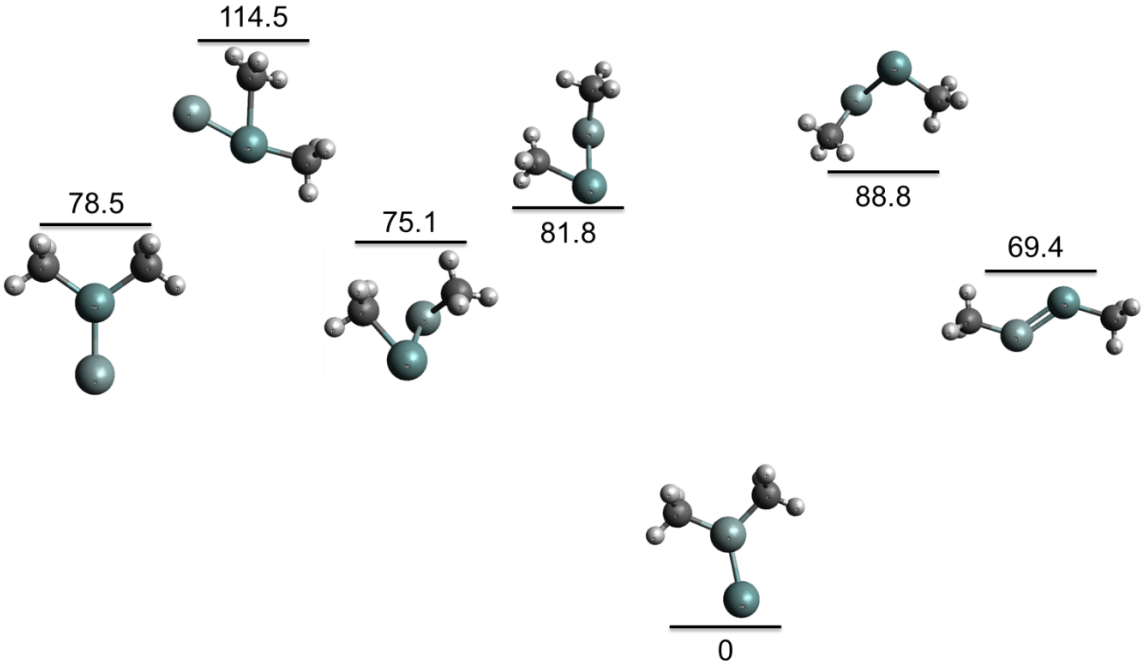

Figure 24: Energy profile for the isomerisation of $SiGeMe_2$, with internal energies given.

A transition state connecting SiGeGS1 and SiGeGS2 has not yet been found. Interestingly, a second doubly bridged structure corresponding to a stable minimum (SiGeGS4) could be identified, with the relevant section of the energy profile shown in Figure 25.

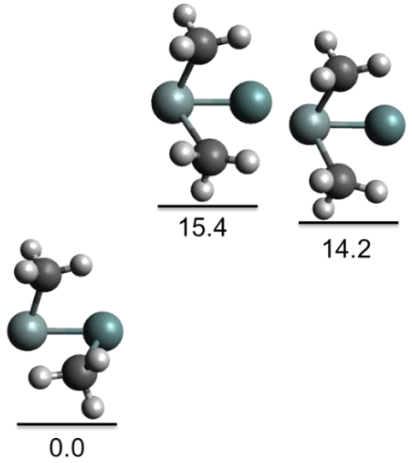

Figure 25: Energy profile for the isomerisation of SiGeGS2 to SiGeGS4, with internal energies given.

The barrier for the isomerisation of the species on the right is with 1.2 kJ/mol very small and corresponds to a rotation of the methyl group by 60°. The methyl groups are located closer to silicon than germanium with a Ge-Si-C angle of 66.8° and the hydrogen atoms oriented towards the germanium atom. Furthermore, Figure 26 shows the results from

an AIM analysis on the wavefunction obtained at the RB3LYP/6-311G(2df,p) level of theory.[43] Large correlation-consistent basis sets could not be used because of the regrettable restriction of the author to the free version, where a maximum of 400 primitive gaussians is supported. The charges again support the electrostatic interpretation of the bridged structures. No bond critical point has been found between carbon and germanium. The Si-Ge AIM bond order was found to be 1.49.

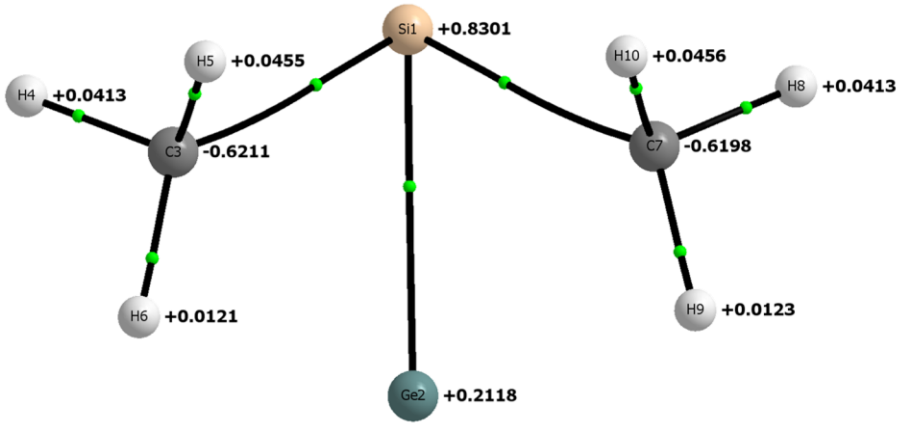

Figure 26: Bond paths, bond critical points and charges obtained from AIM analysis.

Several 2D Scans were performed, with a representative result shown below in Figure 27.

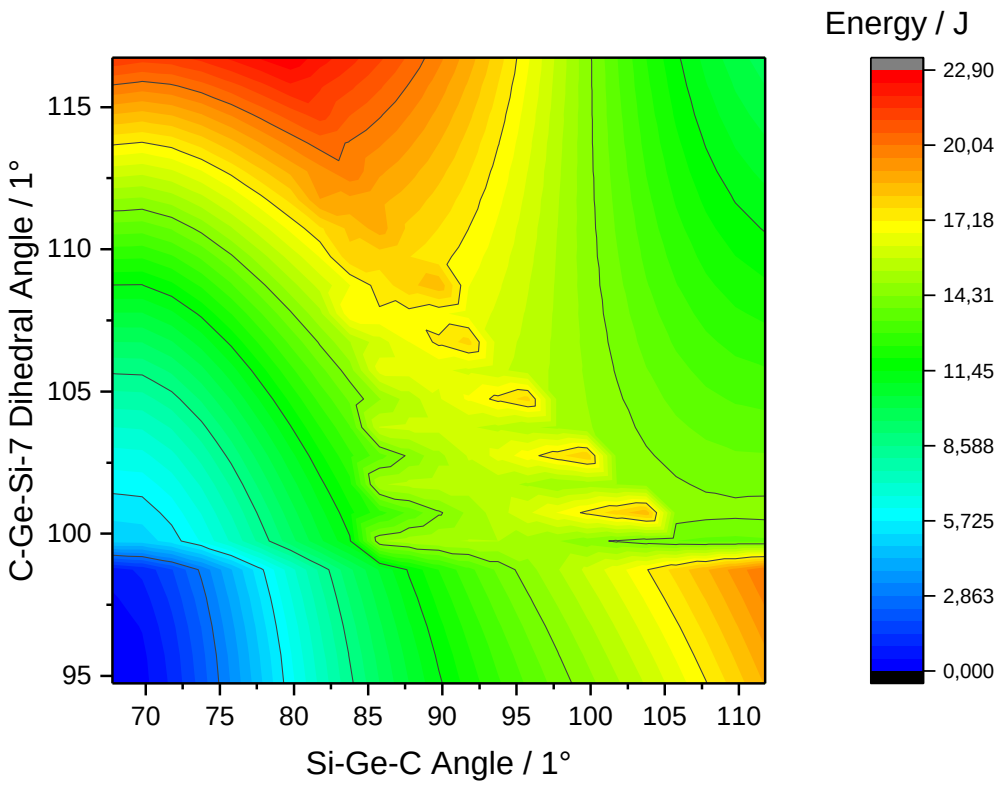

Figure 27: 2D relaxed scan with fixed CH_3 group geometry.

Geometries of the tipping points at the region in the middle of the plot were used as input structure for TS searches, though none of the latter yielded satisfactory results. Additionally, the results of a more sophisticated 2D scan with only C-H bond lengths fixed is shown in Figure 28.

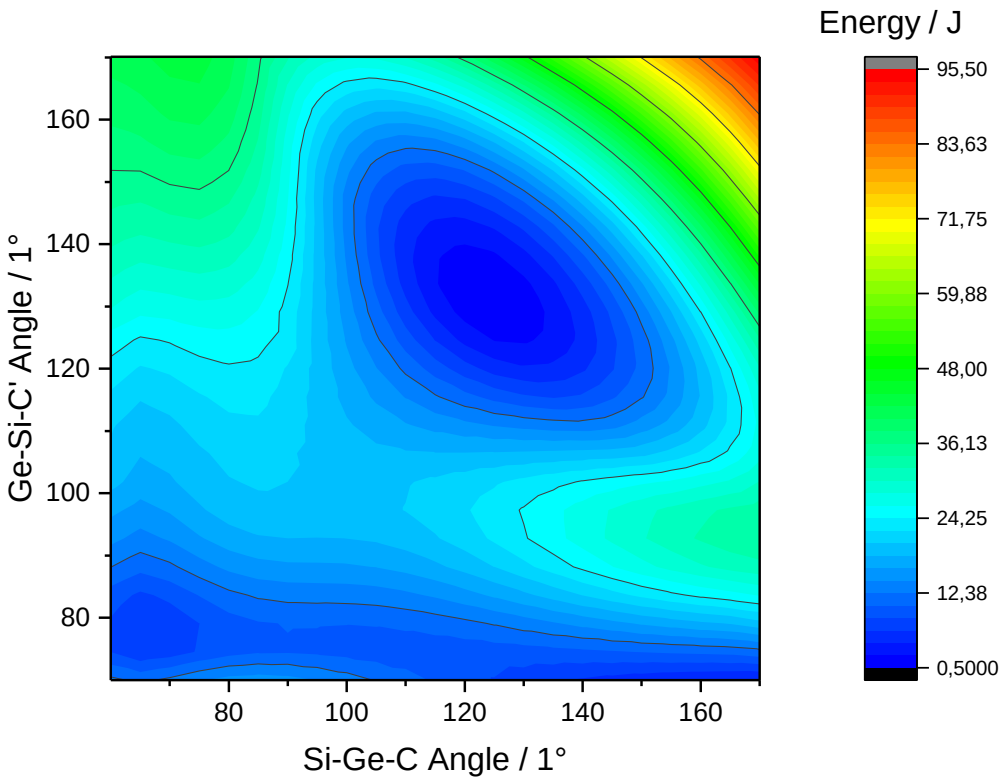

Figure 28: 2D relaxed scan with fixed C-H bond length.

The region of the bridged structure is clearly apparent at the bottom left corner, whereas the trans-bent structure is located at the prominent hollow where both angles are close to 130°. A long shallow channel eventually leading to SiGeGS3 is also discernible.

Only one minimum is visible in the bottom left corner owing to the low angular resolution. Additionally, the coordinate driven methods are usually distorted towards the scan direction because the intrinsic reaction coordinate is replaced with only one internal coordinate (or two, in the case of the two-dimensional scans) like an angle or bond length, which is then gradually increased and the structure reoptimized. The absence of the at least two expected minimum structures in the doubly bridged region is therefore not surprising.

3.2.1.3 Germanium-Germanium

Ge-Ge bond length and Ge-Ge-C angle in the trans-bent Ge_2Me_2 species deviate less than 2% from the MP2 geometries given in the literature.[46] The obtained energy profile is given in Figure 29.

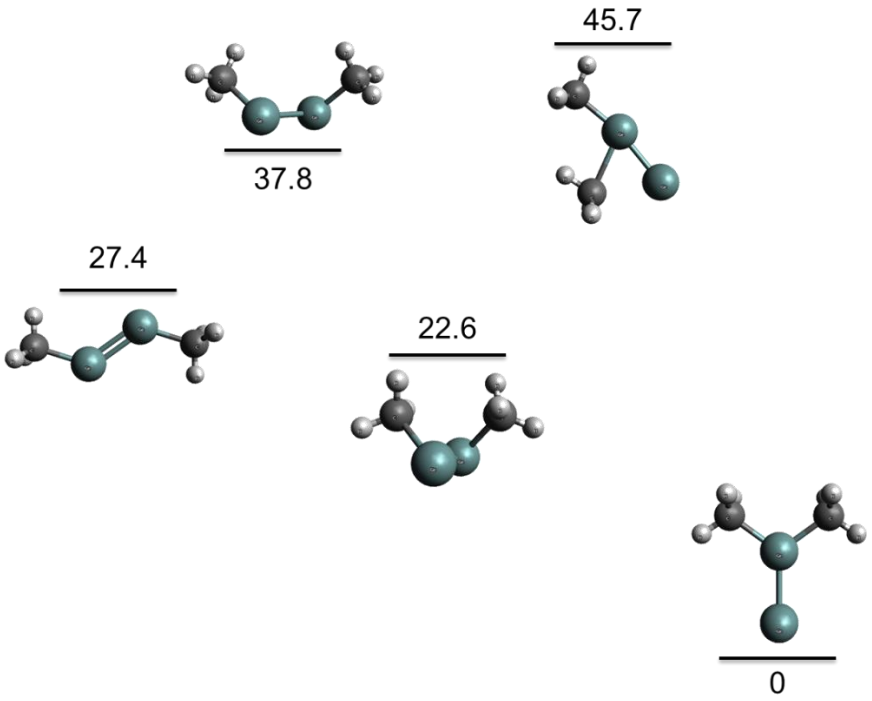

Figure 29: Energy profile for the isomerisation of Ge_2Me_2, with internal energies given.

The doubly bridged species is energetically favoured with respect to the trans-bent structure, so the relative energetical order is inverted when passing from Si_2Me_2 to Ge_2Me_2.

3.2.2 Isomers of $E_2(CF_3)_2$

Within the level of theory deployed, a trans-bent structure was not found. Selected geometrical quantities for the bridged isomer of $E_2(CF_3)_2$ are listed in Table 6. For the heteronuclear species, the second angle given is the Si-Ge-C angle.

Table 6: Selected geometrical parameters of $E_2(CF_3)_2$ isomers.

System	C-E-E-C Dihedral	E-E-C Angle	E-E Bond
SiSiGS2	96.4°	77.8°	2.457 Å
SiGeGS2	96.1°	79.7° / 75.8°	2.534 Å
GeGeGS2	95.9°	77.6°	2.609 Å

The observed change in the two angles is negligible when interchanging silicon with germanium, only the bond lengths are found to be remarkably long. Even the Si-Si bond with the CF_3 substituents is longer than the Ge-Ge bond in Ge_2Me_2. Nevertheless, the relative elongation of the E-E bond is comparable and about 6.2% for both CH_3 and CF_3 when going from SiSiGS2 to GeGeGS2.

For comparison with the E_2Me_2 system, Table 7 shows selected geometrical parameters for the investigated vinylidene structures.

Table 7: E-E bond length and E-E-C angle in vinylidene isomers, comparison of substituents.

Substituent	System	E-E-C Angle	E-E Bond
CH_3	SiSiGS3	124.3°	2.213 Å
	SiGeGS3	124.6°	2.279 Å
	GeSiGS3	125.5°	2.254 Å
	GeGeGS3	125.7°	2.322 Å
CF_3	SiSiGS3	124.8°	2.216 Å
	SiGeGS3	125.1°	2.283 Å
	GeSiGS3	126.2°	2.256 Å
	GeGeGS3	126.4°	2.325 Å

Although there are only few changes, an overall trend towards larger E-E-C angles and E-E bond lengths is visible. The most pronounced differences in Table 6 and Table 7 are those in the E-E bond length, whereas angles are changing much less as has been observed for the E_2Me_2 species. The influence of the CF_3 group on geometry prevails compared to the difference between Si and Ge substitution patterns.

Like for the methyl substituted vinylidene isomers, natural bond orbital analysis was performed for the remote silicon or germanium atom, with the orbital contributions listed in Table 8.

Table 8: Atomic orbital contributions / hybridization for remote Si or Ge from NBO analysis.

System / Atom	E-E Bond 1	E-E Bond 2	Lone Pair
SiSiGS3 / Si	$s^{0.12}p^{0.88}$	$s^{0.00}p^{1.00}$	$s^{0.89}p^{0.11}$
SiGeGS3 / Ge	$s^{0.09}p^{0.90}$	$s^{0.00}p^{1.00}$	$s^{0.91}p^{0.09}$
GeSiGS3 / Si	$s^{0.10}p^{0.89}$	$s^{0.00}p^{1.00}$	$s^{0.91}p^{0.09}$
GeGeGS3 / Ge	$s^{0.08}p^{0.92}$	$s^{0.00}p^{1.00}$	$s^{0.93}p^{0.08}$

Similar trends as already discussed for E_2Me_2 in Table 5 are found. The lone pair for the $E_2(CF_3)_2$ systems have slightly more s- and the σ-bond more p-character. Although the absolute difference is marginal, Bent's rule is therefore followed.[47]

3.2.2.1 Silicon-Silicon

The energy profile obtained for $Si_2(CF_3)_2$ is shown in Figure 30.

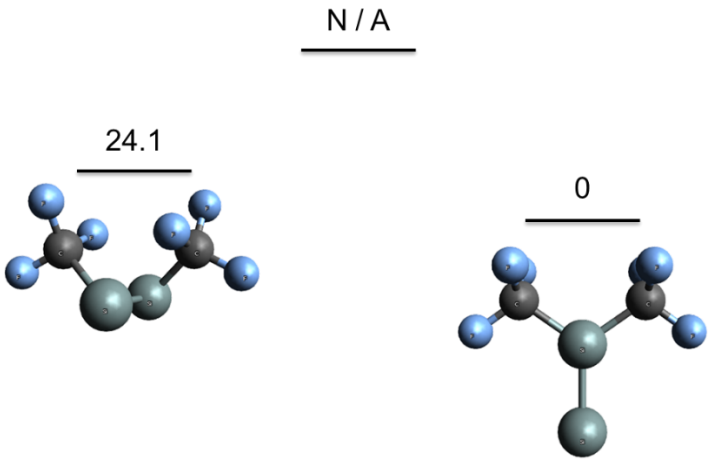

Figure 30: Energy profile for the isomerisation of $Si_2(CF_3)_2$, with internal energies given.

The vinylidene structure is the more stable one, and the energy difference between both structures is about half the value for Si_2Me_2.

Despite numerous and time-consuming attempts, a transition state connecting the SiSiGS2 and SiSiGS3 has not yet been found. Instead, several at first sight promising transition state structures were found to correspond to fluoride transfer to silicon or germanium. As two characteristic examples may serve the results of IRC calculations shown on the following pages in Figure 31 and Figure 32.

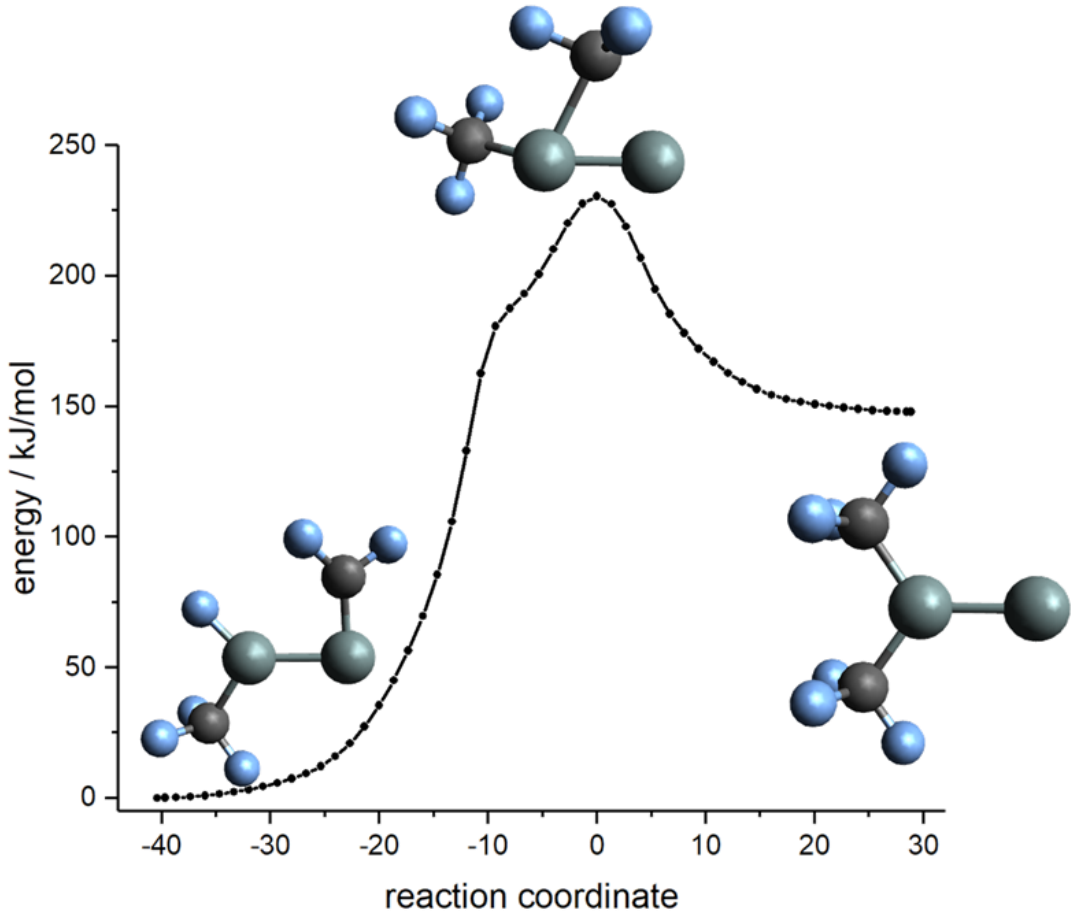

Figure 31: IRC for the decomposition / fluoride transfer starting from SiSiGS3 together with optimized structures.

At first sight, a transition state similar to the ones found for GeSiTS23 and GeGeTS23 was obtained. Following the IRC, at point −9 occurred fluoride transfer to silicon, and the structure at the bottom left of Figure 31 is found. This structure is by 148.0 kJ/mol more stable than the vinylidene structure SiSiGS3 and separated from it by a barrier of 82.5 kJ/mol. The barrier is situated between the two barriers for the isomerisation of SiSiGS3 and SiGeGS3 to their corresponding bridged structure.

The decomposition product is much more stable than the vinylidene structure. Indeed, many of the problems faced in this work resulted from a number of undesired minimum or transition state structure. To sum it all up, trying to describe the desired isomerisation of $E_2(CF_3)_2$ is like balancing a sphere over a slippery, narrow ridge.

Another illustrative case with two fluoride atoms transferred is shown in Figure 32.

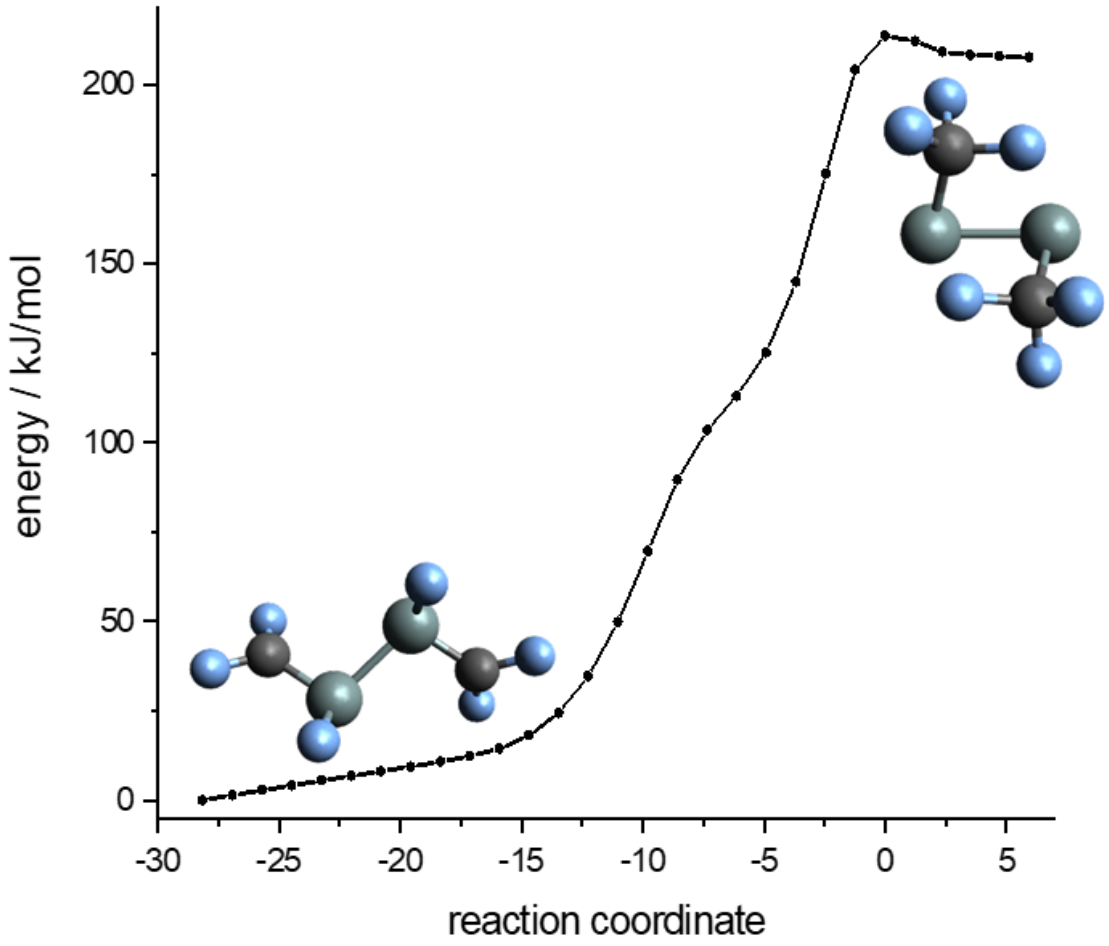

Figure 32: IRC for the decomposition / fluoride transfer starting from SiSiGS2 together with optimized structures.

The barrier to this decomposition is with 6.0 kJ/mol very small, and the decomposition product shown in the bottom left corner is more stable than SiSiGS2 by 225.8 kJ/mol. The energetic distance between this species and SiSiGS3 is therefore as large as 201.7 kJ/mol.

Due to numerous and obvious reasons, CF_3 groups are unsuitable substituents and $Si_2(CF_3)_2$ will never be accessible experimentally in relevant amount and concentration. This decomposition is one of the reasons. Nevertheless, the investigation was not doomed to failure in the first place: as explained in the introduction, the use of a broad range of substituents including the most extreme examples is preferable from a theoretical point of view. With this in mind, two of the decomposition pathways are only presented here because in this case they were so dominant that is was not yet possible to find a structure for SiSiTS23.

3.2.2.2 Silicon-Germanium

The energy profile for the isomerization of $SiGe(CF_3)_2$ is shown in Figure 33.

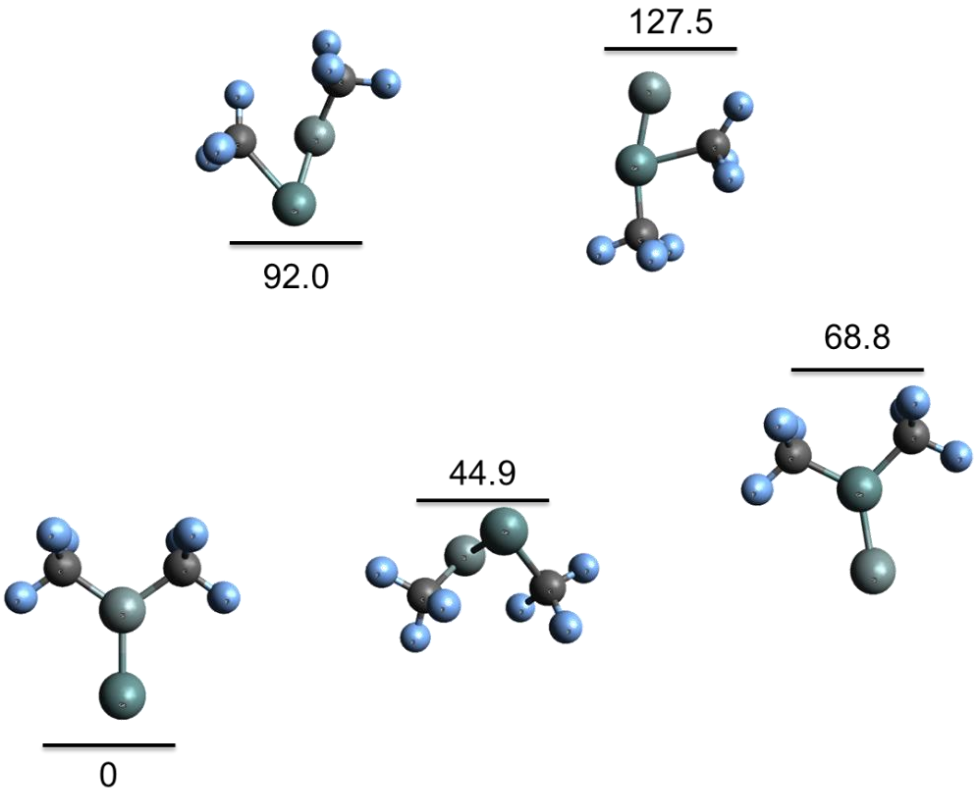

Figure 33: Energy profile for the isomerisation of $SiGe(CF_3)_2$, with internal energies given.

The barriers involved in the isomerisation of SiGeGS2 to the two possible products and the energy difference between the latter are listed in Table 9 together with the values obtained for the E_2Me_2 system.

Table 9: Comparison of barriers and energy differences for the two substitution patterns.

Energy parameter	Value / kJ/mol	
	$SiGeMe_2$	$SiGe(CF_3)_2$
SiGeGS2 → SiGeGS3 Barrier	6.7	47.1
SiGeGS2 → GeSiGS3 Barrier	39.4	82.6
GeSiGS3 – SiGeGS3 Difference	78.0	68.8

In both cases, the vinylidene species with the silicon atom connected to the two substituents is thermodynamically and kinetically favoured. A very rough estimate of the product ratio can be obtained using either the Boltzmann distribution (thermodynamic

ratio) or the Eyring-Polanyi (kinetic ratio) equation.[30] The thermodynamic (kinetic) SiGeGS3/GeSiGS3 ratio for $SiGeMe_2$ is found to be 59 (0.32) times the ratio for $SiGe(CF_3)_2$. Absolute values of these ratios lie between 10^6 and 10^{14} and indicate almost exclusively the formation of the SiGeGS3 species, but absolute values of this type tend to be erroneous and should be used with caution. It should always be kept in mind that these reactions are highly hypothetical, as side reactions like fluoride transfer or oligomerization and important effects like those of entropical nature are completely neglected.

3.2.2.3 Germanium-Germanium

The energy profile for the isomerization of $GeGe(CF_3)_2$ is shown in Figure 34.

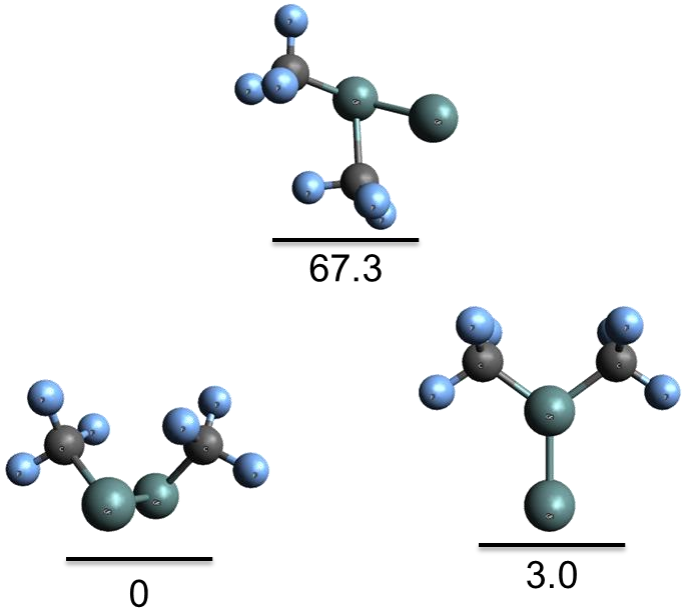

Figure 34: Energy profile for the isomerisation of $GeGe(CF_3)_2$, with internal energies given.

The doubly bridged structure is slightly more stable than the vinylidene, at least at this level of theory. Like in the other cases, the barrier is much larger than for E_2Me_2, whereas differences in energy between minimum structures are smaller.

At this point it would be interesting whether the trend is continued when passing on to tin or lead. Relativistic effects become more and more important for these elements. Therefore corrections would have to be incorporated, either by effective core potentials or explicit relativistic calculations.[30,31]

3.3 Triplet State Calculations

It has been reported that the energy of triplet states may be significantly lowered by electronegative groups.[20] Therefore quick calculations of triplet states were performed at the UB3LYP/cc-pVTZ level of theory. Besides trans-bent and vinylidene species, twisted cis-bent structures were found, *ergo* the doubly bridged structures are widened so that the E-E-C angles exceed 90°.

3.3.1 Minimum Structures of $E_2(CH_3)_2$

The energies referenced to the lowest value within any set of isomers are given in Table 10 together with the adiabatic singlet-triplet-splitting (between optimized structures) and the expectation value of the total spin squared.

Table 10: Expectation value for $\boldsymbol{S^2}$, internal energy for the triplet state and singlet-triplet splitting for E_2Me_2.

System	$\langle S^2 \rangle / \hbar^2$	E / kJ/mol	ΔE_{S-T} / kJ/mol
SiSiGS1	2.0087	28.4	7.1
SiSiGS2	2.0097	64.1	26.5
SiSiGS3	2.0071	0.0	12.0
SiGeGS1	2.0070	60.1	1.8
SiGeGS2	2.0036	87.1	23.1
SiGeGS3	2.0043	0.0	11.1
GeSiGS3	2.0061	82.0	26.5
GeGeGS1	2.0058	11.5	−3.1
GeGeGS2	2.0040	39.1	29.3
GeGeGS3	2.0034	0.0	12.8

The values for $\langle S^2 \rangle$ are close to 2 $\hbar^2$, therefore spin contamination is negligible. Energies for SiSi and SiGe species are comparable on singlet and triplet PES, only the energetic order of GeGeGS1 and GeGeGS2 is interchanged. The singlet-triplet splitting is small, and for trans-bent Ge_2Me_2 the triplet state is even found to be favourable. Therefore, the potential energy surfaces have to intersect at some point. Because the difference between electronic states and the nuclear motion described by the PES becomes small, their coupling cannot be neglected anymore, and the Born-Oppenheimer-approximation

breaks down.[30] Treating such effects rigorously is tempting, but beyond the scope of this rather trivial course. For the trans-bent structures, the energy of the triplet state is lowered relative to the singlet state when substituting Si with Ge. This seems to go along with the concept of charge-shift-bonds, an intermediate bonding pattern between covalent and ionic.[48–51] Whereas carbon-carbon double bonds are usually interpreted as being exclusively covalent, this is not the case for heavier multiple bonds, which exhibit diradical character or the mentioned charge-shift bonding.[44] Triplet states may be favourable due to exchange energy, but require excitation energy for entirely paired electrons. This is not the case for species with charge-shift or diradical multiple bonding.

3.3.2 Minimum Structures of $E_2(CF_3)_2$

The energies referenced to the lowest value within any set of isomers are given in Table 11 together with the adiabatic singlet-triplet-splitting (between optimized structures) and the expectation value of the total spin squared.

Table 11: Expectation value for $\boldsymbol{S^2}$, internal energy for the triplet state and singlet-triplet splitting for $E_2(CF_3)_2$.

System	$\langle S^2 \rangle / \hbar^2$	E / kJ/mol	$\Delta E_{S\text{-}T}$ / kJ/mol
SiSiGS1	2.0093	5.7	/
SiSiGS2	2.0045	41.0	39.7
SiSiGS3	2.0080	0.0	22.8
SiGeGS1	2.0073	32.3	/
SiGeGS2	2.0042	69.3	46.7
GeSiGS2	2.0037	59.8	37.2
SiGeGS3	2.0052	0.0	22.3
GeSiGS3	2.0063	69.1	22.6
GeGeGS1	2.0059	0.0	/
GeGeGS2	2.0036	28.2	43.6
GeGeGS3	2.0036	8.8	21.2

The values for $\langle S^2 \rangle$ are close to 2 $\hbar^2$, therefore spin contamination is negligible. Unlike as for the singlet state, trans-bent structures were found to be stable minima. GeGeGS1 is even the global minimum on the triplet PES (neglecting decomposition).

There were two different structures found for the GS2 species, with the corresponding section of the energy profile shown in Figure 35.

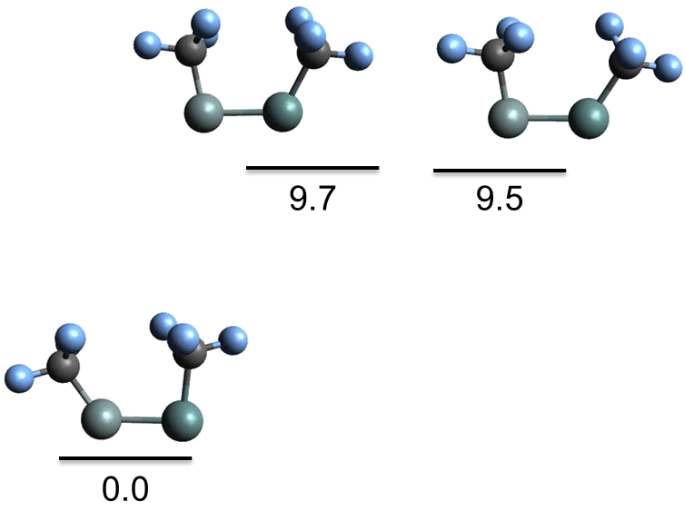

Figure 35: Energy profile for the isomerisation of triplet $SiGe(CF_3)_2$, with internal energies given.

The small barrier of only 0.24 kJ/mol was not found for the other calculations in this work so far. Only for the bridged structure of $SiGeMe_2$, a second form resulting from CH_3 rotation was found. Either the structure on the right in Figure 35 is no longer a true minimum for the other cases, or the barrier is so small that it is easily overstepped. Because the bridged structures of all homonuclear were found to have C_2 symmetry, it is relatively safe to say that only one bridged minimum exists.

4 Conclusions and Outlook

It became clear after several trial runs that the originally intended theoretical study on the redox induced substituent shift in heavy multiple bonds is too complex to be conducted in time. However, during the preliminary calculations, several unprecedented structures were found, especially for borole, NHB and NHC substituents. The electronic structure leading to these unusual geometries is an interesting topic for further investigation, especially with focus on careful population and orbital analysis. Generation of accurate wavefunctions including correlated methods beyond the Kohn-Sham-reference should precede those analyses. The phosphorus species shown in Figure 12 is interesting not only concerning its electronic structure, but also with respect to Ge_2 and heteronuclear substitution patterns.

The methylene bridged diphenyl species is even appealing from an experimentalists point of view, as similar compounds may be accessible with sterically more demanding groups.

Stable geometries of E_2CH_3 and E_2CF_3 were described in detail, together with the isomerisation between them. Some of these species are well described in the literature, but exhaustive calculations on most of them are scarce. Out of the one- and two-dimensional scans performed in this work, the scans of two angles starting from a doubly bridged structure were the most useful. Although computationally very demanding, they provide valuable insight into an appropriate subset of the hypersurface that is intuitively comprehensible and should therefore be pursued in future work on this topic. The geometries obtained at the RB3LYP level of theory with medium sized basis set seem to be reliable. Nevertheless, more sophisticated correlated calculations for the sake of accurate energies are desirable, at least as single point calculations on top of the RB3LYP geometries.

It should be noted in particular that the differences between methyl and trifluoromethyl substituents are comparatively large, with the latter not even having a trans-bent structure as stable minimum. Hence, it would be reasonable to extend the calculations on species being partially fluorinated or bearing two different substituents like $E_2CF_3CH_3$. This would naturally result in both an increased complexity of the system and a more thorough understanding of it.

Furthermore, rough calculations on triplet state geometries were also presented. These indicate that a closer look to singlet-triplet splitting and non-adiabatic coupling might be rewarding, as conical intersections – for example in the twist / doubly bridged region – are anticipated. Care must be taken as the results presented in Table 3 indicate that UB3LYP may be inappropriate, and the splitting between singlet and triplet states thus much larger in reality.

In all cases except $Ge_2(CF_3)_2$, the vinylidene species is the global minimum, at least when neglecting collapse of the substituent. The bridged structures are particular interesting and less well investigated. E-E-C angles in these are found to be smaller than 90° for singlet states and larger than 90° for triplet states an dianions.

5 Bibliography

[1] C. Präsang, D. Scheschkewitz, *Chem. Soc. Rev.* **2016**, *45*, 900–921.

[2] A. Jana, V. Huch, D. Scheschkewitz, *Angew. Chemie* **2013**, *125*, 12401–12404.

[3] X. Lu, L. Shi, J. Ming, *Arab. J. Chem.* **2016**, *9*, 163–169.

[4] X.-H. Lu, H.-B. Yu, Y.-H. Xu, W.-R. Wu, *Chinese J. Chem.* **2006**, *24*, 307–310.

[5] S. Huo, X. Li, Y. Zeng, S. Zheng, L. Meng, *J. Mol. Model.* **2013**, *19*, 3501–3506.

[6] X. Lu, L. Shi, W. Bao, D. Liu, *Comput. Theor. Chem.* **2013**, *1022*, 75–81.

[7] M. Karni, Y. Apeloig, *Silicon Chem.* **2002**, *1*, 59–65.

[8] N. Takagi, S. Nagase, *J. Organomet. Chem.* **2007**, *692*, 217–224.

[9] J. P. Wagner, P. R. Schreiner, *J. Chem. Theory Comput.* **2016**, *12*, 231–237.

[10] K. Kobayashi, S. Nagase, *Organometallics* **1997**, *16*, 2489–2491.

[11] T. Szilvási, T. Veszprémi, *Organometallics* **2012**, *31*, 3207–3212.

[12] A. Sekiguchi, *Science (80-.).* **2004**, *305*, 1755–1757.

[13] A. Sekiguchi, M. Ichinohe, R. Kinjo, *Bull. Chem. Soc. Jpn.* **2006**, *79*, 825–832.

[14] R. Kinjo, M. Ichinohe, A. Sekiguchi, *J. Am. Chem. Soc.* **2007**, *129*, 26–27.

[15] K. Takeuchi, M. Ichinohe, A. Sekiguchi, *J. Am. Chem. Soc.* **2008**, *130*, 16848–16849.

[16] K. Takeuchi, M. Ikoshi, M. Ichinohe, A. Sekiguchi, *J. Am. Chem. Soc.* **2010**, *132*, 930–931.

[17] A. Rit, J. Campos, H. Niu, S. Aldridge, *Nat. Chem.* **2016**, *8*, 1022–1026.

[18] C. Hansch, A. Leo, R. W. Taft, *Chem. Rev.* **1991**, *91*, 165–195.

[19] M.-J. Cheng, H.-M. Cheng, S.-Y. Chu, *J. Phys. Chem. A* **2006**, *110*, 10495–10500.

[20] M. R. Momeni, F. A. Shakib, *Organometallics* **2011**, *30*, 5027–5032.

[21] J. P. Malrieu, G. Trinquier, *J. Am. Chem. Soc.* **1989**, *111*, 5916–5921.

[22] G. Trinquier, J. paul Malrieu, *J. Am. Chem. Soc.* **1987**, *109*, 5303–5315.

[23] E. A. Carter, W. A. Goddard, *J. Phys. Chem.* **1986**, *90*, 998–1001.

[24] M. Lein, A. Krapp, G. Frenking, *J. Am. Chem. Soc.* **2005**, *127*, 6290–6299.

[25] S. Nagase, K. Kobayashi, N. Takagi, *J. Organomet. Chem.* **2000**, *611*, 264–271.

[26] H. Jacobsen, *Chem. - A Eur. J.* **2010**, *16*, 976–987.

[27] Gaussian 09, Revision A.02, M. J. Frisch, G. W. Trucks, H. B. Schlegel, G. E. Scuseria, M. A. Robb, J. R. Cheeseman, G. Scalmani, V. Barone, G. A. Petersson, H. Nakatsuji, X. Li, M. Caricato, A. Marenich, J. Bloino, B. G. Janesko, R. Gomperts, B. Mennucci, H. P. Hratchian, J. V. Ortiz, A. F. Izmaylov, J. L. Sonnenberg, D. Williams-Young, F. Ding, F. Lipparini, F. Egidi, J. Goings, B. Peng, A. Petrone, T. Henderson, D. Ranasinghe, V. G. Zakrzewski, J. Gao, N. Rega, G. Zheng, W. Liang, M. Hada, M. Ehara, K. Toyota, R. Fukuda, J. Hasegawa, M. Ishida, T. Nakajima, Y. Honda, O. Kitao, H. Nakai, T. Vreven, K. Throssell, J. A. Montgomery, Jr., J. E. Peralta, F. Ogliaro, M. Bearpark, J. J. Heyd, E. Brothers, K. N. Kudin, V. N. Staroverov, T. Keith, R. Kobayashi, J. Normand, K. Raghavachari, A. Rendell, J. C. Burant, S. S. Iyengar, J. Tomasi, M. Cossi, J. M. Millam, M. Klene, C. Adamo, R. Cammi, J. W. Ochterski, R. L. Martin, K. Morokuma, O. Farkas, J. B. Foresman, and D. J. Fox, Gaussian, Inc., Wallingford CT, **2016**.

[28] H. Jacobsen, T. Ziegler, *J. Am. Chem. Soc.* **1994**, *116*, 3667–3679.

[29] S. Koseki, M. S. Gordon, *J. Phys. Chem.* **1989**, *93*, 118–125.

[30] F. Jensen, *Introduction to Computational Chemistry*, John Wiley & Sons, Inc., West Sussex, **2007**.

[31] D. C. Young, *Computational Chemistry*, John Wiley & Sons, Inc., New York, USA, **2001**.

[32] NBO Version 3.1, E. Glendening, A. E. Reed, J. E. Carpenter, F. Weinhold.

[33] P. Atkins, R. Friedman, *Molecular Quantum Mechanics*, Oxford University Press, New York, **2011**.

[34] D. Seyferth, R. E. Mammarella, *J. Organomet. Chem.* **1978**, *156*, 279–297.

[35] D. J. D. Wilson, S. A. Couchman, J. L. Dutton, *Inorg. Chem.* **2012**, *51*, 7657–7668.

[36] “CASSCF,” can be found under www.gaussian.com/CAS, **2017**.

[37] Y. Wang, Y. Xie, P. Wei, R. B. King, H. F. Schaefer, P. von R. Schleyer, G. H. Robinson, *Science (80-.).* **2008**, *321*, 1069–1071.

[38] N. Holzmann, D. M. Andrada, G. Frenking, *J. Organomet. Chem.* **2015**, *792*, 139–148.

[39] K. C. Mondal, S. Roy, B. Maity, D. Koley, H. W. Roesky, *Inorg. Chem.* **2016**, *55*, 163–169.

[40] M. I. Arz, M. Straßmann, A. Meyer, G. Schnakenburg, O. Schiemann, A. C. Filippou, *Chem. - A Eur. J.* **2015**, *21*, 12509–12516.

[41] B. S. Thies, R. S. Grev, H. F. Schaefer, *Chem. Phys. Lett.* **1987**, *140*, 355–361.

[42] B. T. Colegrove, H. F. Schaefer, *J. Am. Chem. Soc.* **1991**, *113*, 1557–1561.

[43] AIMAll Version 17.01.25, T. A. Keith, TK Gristmill Software, **2017**.

[44] Y. Jung, M. Brynda, P. P. Power, M. Head-Gordon, *J. Am. Chem. Soc.* **2006**, *128*, 7185–7192.

[45] A. J. Bridgeman, L. R. Ireland, *Polyhedron* **2001**, *20*, 2841–2851.

[46] T. L. Allen, W. H. Fink, P. P. Power, *J. Chem. Soc. Dalt. Trans.* **2000**, 407–412.

[47] I. V. Alabugin, S. Bresch, G. dos Passos Gomes, *J. Phys. Org. Chem.* **2015**, *28*, 147–162.

[48] A. Shurki, P. C. Hiberty, S. Shaik, *J. Am. Chem. Soc.* **1999**, *121*, 822–834.

[49] E. Ploshnik, D. Danovich, P. C. Hiberty, S. Shaik, *J. Chem. Theory Comput.* **2011**, *7*, 955–968.

[50] S. Shaik, P. Maitre, G. Sini, P. C. Hiberty, *J. Am. Chem. Soc.* **1992**, *114*, 7861–7866.

[51] S. Shaik, D. Danovich, W. Wu, P. C. Hiberty, *Nat. Chem.* **2009**, *1*, 443–449.